ChemCatChem

Review
doi.org/10.1002/cctc.202301391

Chemistry Europe
European Chemical Societies Publishing

www.chemcatchem.org

Manganese(I) Catalyzed CO_2 Reduction Processes in Homogenous Phase

Sylwia Kostera[a] and Luca Gonsalvi*[a]

This review article is dedicated to Dr. Francesco Vizza (CNR-ICCOM), a colleague and a friend, in recognition of his outstanding contribution to chemistry and catalysis, on occasion of his retirement.

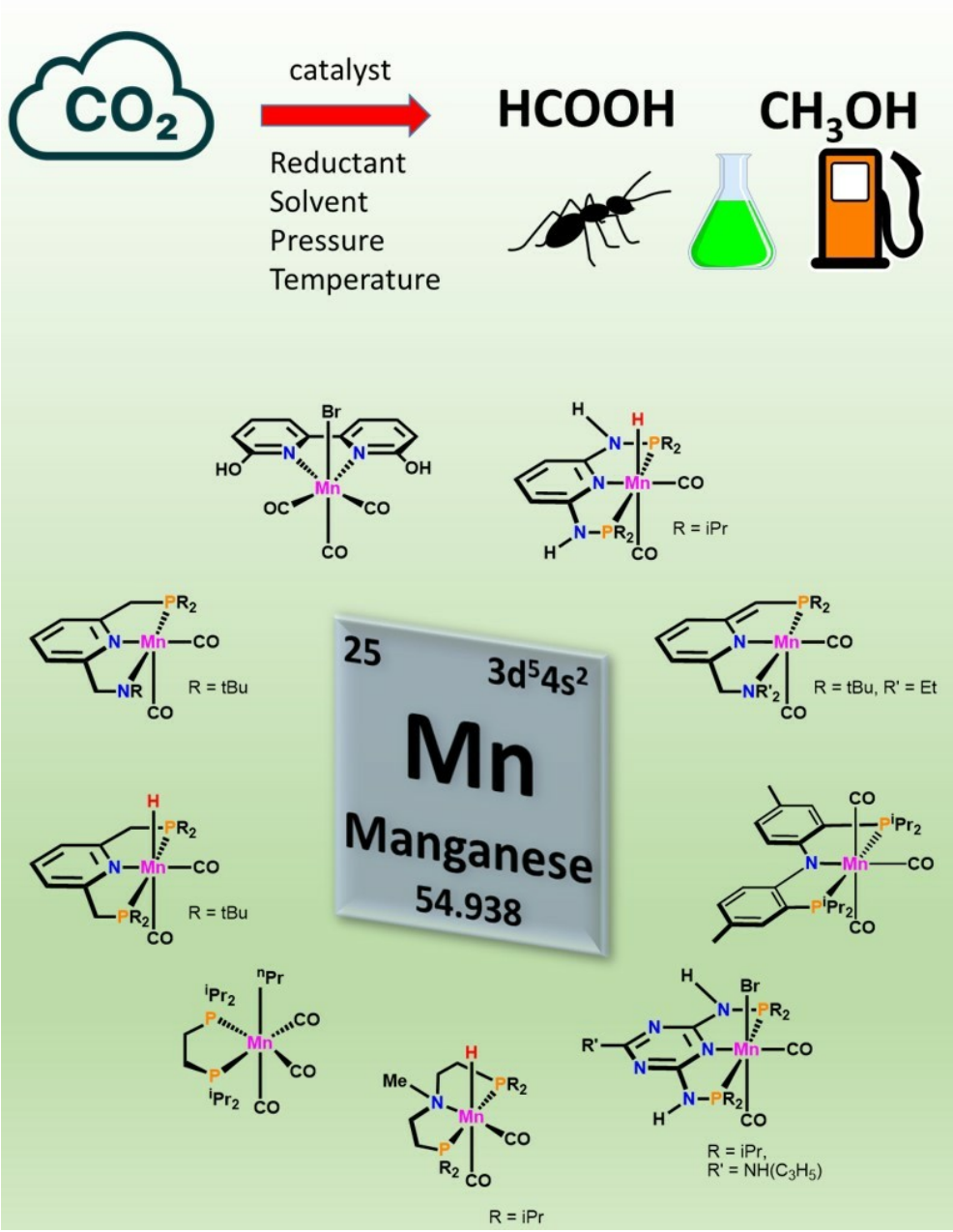

The catalytic activation of carbon dioxide (CO_2) can be a promising tool for the use of this abundant, non-flammable and non-toxic gas as feedstock for C1 chemical synthesis, in particular for bulk products such as formic acid (HCOOH) and methanol (CH_3OH). The key for successful, widespread use of CO_2 is the design and application of efficient, thermally robust and cheap catalysts. In the last decade, the use of earth-abundant transition metal complexes, in particular those of 3d metals, has shown promising results. In this review article, a comprehensive summary of the main catalytic systems described in the literature for homogeneous Mn(I)-catalyzed CO_2 reduction processes (hydrogenation, hydroboration and hydrosilylation) will be described, with particular attention to the effect of stabilizing ligands, reaction conditions and need for additives, together with mechanistic details often obtained by a combination of experimental data and DFT calculations.

1. Introduction

In the quest for more sustainable and environmentally friendly approaches to chemical synthesis, scientists are facing various issues, among which the choice of abundant substrates, mild conditions, high process efficiency and selectivity to the desired products, use of green solvents etc. Many industrial processes, especially those applied for the synthesis of bulk chemicals, still use harsh reaction conditions (high pressures and temperatures) and/or toxic gases such as carbon monoxide (CO), for example in the synthesis of methanol (CH_3OH) or formic acid (HCOOH) from methyl formate. Another environmental issue is the need to curb CO_2 emissions, which have overcome the alert threshold of 400 ppm concentration in the atmosphere, to help in keeping global warming under control. Many research groups have demonstrated over the years the possibility to use CO_2 as abundant, cheap, non-flammable and non-toxic feedstock for C1 chemical synthesis.[1]

CO_2 utilization processes can be principally divided in i) CO_2 addition, either into unsaturated carbon-carbon bonds, such as C=C double bonds (alkenes) and C≡C triple bonds (alkynes), or in highly strained organic molecules containing heteroatoms (epoxides, aziridines), in which case the carbon oxidation state does not change, and ii) CO_2 reduction, ranging from 2 to 8 electrons, leading to HCOOH, HCHO, CH_3OH, CH_4, respectively. These products find applications in the chemical industry both as bulk chemicals and in the synthesis of commodities, and are so far generally obtained from fossil-based feedstocks. Therefore, practical ways to obtain them from CO_2 are highly desired. In order to overcome the thermodynamic stability of CO_2 and promote C=O bond activation for further transformations under feasible reaction conditions, the use of a catalyst is needed. Thus, homogeneous, heterogeneous, photo- and electrocatalysts have been designed, extensively studied and applied for CO_2 utilization processes.[2]

Homogeneous catalysts offer some important advantages, namely easier synthesis by reaction between suitable metal precursors and stabilizing ligands, easier tuning of the steric and electronic properties by simple ligand design, and in general the possibility to achieve higher product selectivity under milder reaction conditions. Traditionally, homogeneously catalyzed CO_2 reduction processes have been the realm of precious metal catalysts, in particular Ru and Ir. With the use of appropriate stabilizing ligands, mainly based on phosphorus and/or nitrogen, extraordinary turnover numbers (TONs) and turnover frequencies (TOFs) have been obtained, for example in CO_2 hydrogenation to HCOOH or formate.[3] The major drawbacks of platinum group metals are however their high costs, and the low abundance in the Earth's crust (Ru: 1×10^{-4} ppm, Ir: 5×10^{-5} ppm),[4] thus for these reasons earth-abundant metals are being studied as possible replacements. In the last decade, complexes of 3d metals such as Fe,[5] Co,[6] and Ni[7] have been studied for CO_2 hydrogenation, and only since 2016 manganese (Mn), the third most abundant metal in the Earth's crust, has received attention for this kind of process. In the present review article, the discussion will be focused on the state-of-the-art for homogeneous Mn(I)-catalyzed CO_2 reduction processes. Thus, heterogeneous, photo- and electrocatalytic approaches will not be included. The literature data will be grouped based on the type of reaction. CO_2 hydrogenation was reported either as direct (Scheme 1a), i.e. the conversion of CO_2/H_2 gas mixtures to HCOOH, formates or CH_3OH, and indirect hydrogenation to CH_3OH (Scheme 1b), that involves the use of amines or alcohols as shuttles to obtain formamides or esters, and the following hydrogenation of these intermediates to the desired product. Next, CO_2 hydroboration processes, leading to boryl-protected HCOOH, HCHO and CH_3OH will be highlighted, showing how ligand effects and tuning of the reaction conditions can affect the process selectivity (Scheme 1c). Then, in the following section the few existing reports on Mn-catalyzed CO_2 hydrosilylation processes will be summarized, focusing on the proposed reaction mechanisms leading to silylformates, bis(silyl)acetals and methoxysilanes (Scheme 1d).

2. CO_2 hydrogenation

CO_2 hydrogenation can be formally described as the addition of hydrogen (H_2) to CO_2. Depending on the reaction conditions, type of catalyst, use of base or additives such as Lewis acids, and in particular on the partial pressure ratios between CO_2 and H_2, different products can be obtained. In the case of the 2-electrons CO_2 hydrogenation to formic acid (HCOOH) or formate salts ($HCOO^-$), generally run under a 1:1 CO_2/H_2 gas ratio

[a] Dr. S. Kostera, Dr. L. Gonsalvi
Istituto di Chimica dei Composti Organometallici (ICCOM)
Consiglio Nazionale delle Ricerche (CNR)
Via Madonna del Piano 10
50019 Sesto Fiorentino (Firenze), Italy
E-mail: l.gonsalvi@iccom.cnr.it

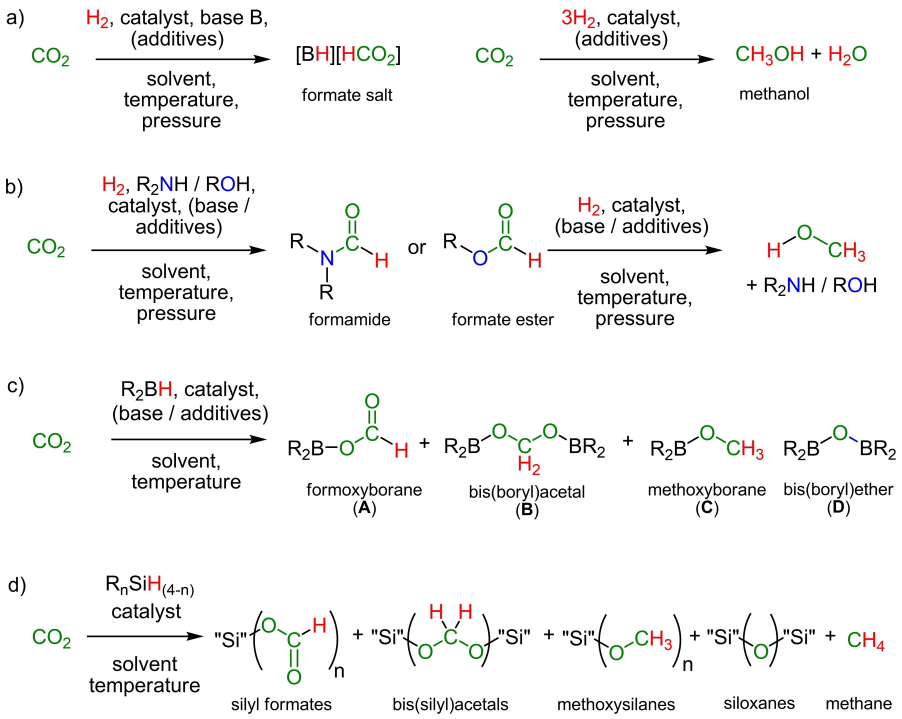

Scheme 1. General scheme of CO_2 reduction processes and possible products.

(Scheme 1a, left), the reaction is endoergonic in gas phase ($\Delta G^\circ = 32.8\ kJ\,mol^{-1}$), mainly due to the large negative entropic factor ($\Delta H^\circ = -31.5\ kJ\,mol^{-1}$, $\Delta S^\circ = -216\ J\,mol^{-1}$). In the presence of an added base, for example NH_3, it can be turned to exoergonic ($\Delta G^\circ = -9.5\ kJ\,mol^{-1}$, $\Delta H^\circ = -84.3\ kJ\,mol^{-1}$, $\Delta S^\circ = -250\ J\,mol^{-1}$), and the formation of the corresponding formate salt constitutes the thermodynamic driving force.[8] In the case of 6-electrons CO_2 hydrogenation to methanol (CH_3OH), the required gas ratio is formally $CO_2/H_2 = 1:3$ (Scheme 1a, right), although in practical tests a higher H_2 partial pressure is often used. The gas-phase reaction is exoergonic ($\Delta G^\circ = -9.5\ kJ\,mol^{-1}$, $\Delta H^\circ = -131\ kJ\,mol^{-1}$, $\Delta S^\circ = -409\ J\,mol^{-1}$), thus addition of base is not required to drive the equilibrium to the desired product.[9]

Beside the "direct" hydrogenation of CO_2 to CH_3OH (Scheme 1a, right), another approach reported in the literature leading to CH_3OH from CO_2 involves two steps, i.e. the initial reduction of CO_2 to HCOOH, that in the presence of an amine or an alcohol is transformed *in situ* into a formamide or formate ester, followed by the hydrogenation of these intermediate products to CH_3OH with regeneration of the amine/alcohol, that are thus used as formyl moiety shuttles (Scheme 1b). This approach is generally indicated as "indirect" CO_2 hydrogenation.

For the purpose of this review article, the literature on Mn-catalyzed CO_2 hydrogenation will therefore be discussed separately in "direct" and "indirect" CO_2 hydrogenations. Table 1 summarizes the main reaction conditions and catalytic results for all the described complexes. Drawings of the molecular

Sylwia Kostera received her Bachelor Degree (2010), Master Degree (2012) and PhD in Chemistry (2017) from the Adam Mickiewicz University Poznań (Poland). She was Postdoctoral Fellow at the University of Wroclaw (Poland) from 2017 to 2018, then moved to CNR-ICCOM Florence (Italy) at first as Postdoctoral NAWA Bekker Programme Fellow (2019), and then as Postdoctoral Fellow on various projects since 2020. Her interests include carbon dioxide hydrogenation and hydroboration, precious and earth-abundant transition metals organometallic chemistry, homogeneous catalysis and study of reaction mechanisms.

Luca Gonsalvi received his Laurea (M.Sc.) in Chemistry (1994) from the University of Parma (Italy) and Ph.D. in Organometallic Chemistry and Catalysis (1999) from The University of Sheffield (UK). He was PDRA at Delft University of Technology (NL) from 1999 to 2001, then joined CNR-ICCOM Florence (Italy) as Researcher, then Senior Researcher (2010–2020) and Research Director (since 2021). He received Habilitations as Full Professor in General and Inorganic Chemistry (2016) and in Industrial Chemistry (2019). His interests include carbon dioxide reduction processes, reversible hydrogen storage in LOHCs, precious and earth-abundant metals organometallic chemistry, homogeneous catalysis in water, study of mechanisms.

Table 1. Summary of main reaction parameters, type of products and best TONs for Mn(I)-catalyzed CO_2 direct hydrogenation.

Catalyst	Amount of cat. [μmol]	H_2/CO_2 Ratio	Solvent	Temp. [°C]	Time [h]	Base	Additives	Type of product	Best TON	Ref.
1a	0.2	1/1	THF/H_2O	100	24	DBU	LiOTf	$HCOO^-$	31600	[12]
1a	1	1/1	THF/H_2O	80	48	DBU	–	$HCOO^-$	8600	[12]
1b	1	1/1	EtOH	80	24	DBU	–	$HCOO^-$	1330	[12]
2a	1	1/1	MeCN	65	24	DBU	–	$HCOO^-$	6250	[13]
2b	5	1/1	MeCN	65	24	DBU	–	$HCOO^-$	17	[13]
2c	5	1/1	MeCN	65	24	DBU	–	$HCOO^-$	18	[13]
2d	5	1/1	MeCN	65	24	DBU	–	$HCOO^-$	20	[13]
2e	5	1/1	MeCN	65	24	DBU	–	$HCOO^-$	161	[13]
3a	5	1/1	MeCN	65	24	DBU	–	$HCOO^-$	1299	[13]
3b	5	1/1	MeCN	65	24	DBU	–	$HCOO^-$	88	[13]
3c	5	1/1	MeCN	65	24	DBU	–	$HCOO^-$	164	[13]
4a	5	1/1	THF	110	60	KOH	–	$HCOO^-$	23	[15]
4b	5	1/1	THF	110	60	KOH	–	$HCOO^-$	6	[15]
5a	5	1/1	THF	100	18	KO^tBu	–	$HCOO^-$	58	[16]
6	5	1/1	THF	100	18	KO^tBu	–	$HCOO^-$	49	[16]
7	5	2/1	THF	80	24	DBU	LiOTf	$HCOO^-$	1988	[17]
8a	40	9/1	Dioxane/EtOH	150	68	–	$Ti(O^iPr)_4$	MeOH	19	[20]
8b	10	32/1	Dioxane/EtOH	150	68	–	$Ti(O^iPr)_4$	MeOH	87	[20]
9a	0.1	3/1	THF/H_2O	145	12	Lys	–	HCOOH	40000	[24]
9b	0.1	3/1	THF/H_2O	145	12	Lys	–	HCOOH	38000	[24]
9c	0.1	3/1	THF/H_2O	145	12	Lys	–	HCOOH	25000	[24]
9d	0.1	3/1	THF/H_2O	145	12	Lys	–	HCOOH	300	[24]
10a	0.1	3/1	THF/H_2O	145	12	Lys	–	HCOOH	43000	[24]
10b	0.02	3/1	THF/H_2O	115	12	Lys	–	HCOOH	230000	[24]
10c	0.02	3/1	THF/H_2O	145	12	Lys	–	HCOOH	45000	[24]
11a	0.3	1/1	THF	110	48	DBU	LiOTf	$HCOO^-$	4200	[26]
11b	0.3	1/1	THF	80	24	DBU	LiOTf	$HCOO^-$	18300	[26]
11c	0.3	1/1	THF	80	24	DBU	LiOTf	$HCOO^-$	270	[26]
11d	0.3	1/1	THF	80	24	DBU	LiOTf	$HCOO^-$	5500	[26]
12	2	1/1	THF	80	72	DBU	LiOTf	$HCOO^-$	3805	[27]

structures of the Mn complexes related to the chapter are shown in Figure 1. Noteworthy, pincer-type complexes are predominant in CO_2 reduction processes. Pincer ligands can impart the ideal geometry, electronic and steric properties to the metal center, and can be easily tuned by synthetic variations of donor atoms and their substituents.

2.1. Direct hydrogenation

Homogeneous CO_2 hydrogenation to HCOOH has been studied by numerous research groups worldwide, traditionally in the presence of platinum group metals (PGMs), in particular Ru and Ir, in combination with organophosphines, bipyridines, cyclic diimines and pincer-type ligands, obtaining outstanding turnover numbers (TON) and turnover frequencies (TOF, h^{-1}).[3b,10] Recent results show that very high productivities (TON = 4650000, TOF = 64593 h^{-1}) can be achieved also with base metals such as Ni in the presence of a stabilizing NP_3 tetradentate ligand.[7]

The first report on Mn(I)-catalyzed CO_2 hydrogenation appeared in the literature in 2016 as a predictive DFT computational study (DFT = density functional theory).[11] The authors studied the energy profile of CO_2 hydrogenation starting from [MnBr(bipy)(CO)$_3$] (bipy = bipyridine), previously reported as an active electrocatalyst for the electrocatalytic reduction of CO_2 in the presence of weak Brønsted acids. In detail, the focus of the

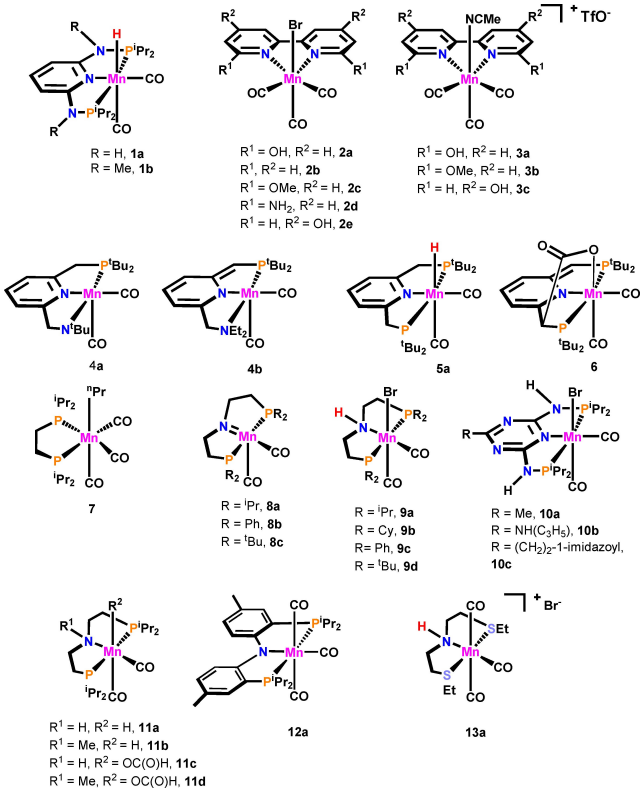

Figure 1. Chemical drawings of Mn(I) homogeneous catalysts used for various CO_2 hydrogenation processes.

investigation was to understand the role of the ratio of σ-donor (PMe_3) and of π-acceptor (CO) ligands in substituted complexes [MnX(bipy)(L_1)(L_2)(CO)] ($L_1 = L_2 = CO$; $L_1 = CO$, $L_2 = PMe_3$; $L_1 = L_2 = PMe_3$; X=CH_3CN) on the rate-limiting step in the catalytic cycle, in the presence of $NH(CH_3)_2$ as base. It was shown that the key steps of the mechanism are heterolytic H_2 cleavage followed by hydride transfer, and that the latter is rate-determining for all the three complexes. It was further demonstrated that this step can be significantly improved by using a proper combination of σ-donor and π-acceptor ligands by subtle ligand tuning, for example replacing PMe_3 with PF_3.

In 2017, the first experimental study on Mn(I)-catalyzed efficient CO_2 hydrogenation to formate was disclosed by Gonsalvi, Kirchner and coworkers.[12] Two well-defined Mn(I) hydridocarbonyl complexes where synthesized from the reaction of [$MnBr(CO)_5$] with 2,6-bis(diaminodiisopropylphosphine)pyridyl pincer type ligands (PNP) and then treated with $LiHBEt_3$. The so-obtained complexes [$MnH(PNP^H$-*i*Pr)$(CO)_2$] (**1 a**) and [$MnH(PNP^{Me}$-*i*Pr)$(CO)_2$] (**1 b**) are structurally similar and differ only by the substituent on the amine N atom in the backbone (H and Me, respectively). They were both tested as catalysts in the presence of DBU (DBU = 1,8-diazabicycloundec-7-ene) as added base, screening the main reaction parameters such as solvent, temperature, pressure, catalyst concentration and need for Lewis acid co-catalysts, showing overall a higher performance of complex **1 a**. The initial test was run at 80 °C in THF/H_2O, 80 bar $H_2/CO_2 = 1:1$, 24 h, using a **1 a**/DBU ratio of 1 : 1000, obtaining (DBUH)(HCO_2) in quantitative yields with TON = 1000. At lower catalyst loadings (**1 a**/DBU = 1 : 10000; [**1 a**] = 0.18 μmol/mL), the yield in formate decreased to 55 %, corresponding to TON = 5520. At a catalyst concentration of 0.036 μmol/mL (**1 a**/DBU = 1 : 50000), TON increased significantly (9100), but lower yields were obtained (16 %). Further optimization showed that by extending the reaction time to 48 h and using a **1 a**/DBU ratio of 1 : 10000, high yields of formate (86 %) and high TON (8600) could be reached. The catalyst performance could be dramatically increased by addition of Li triflate as Lewis acid co-catalysts to the reaction mixture. Addition of LiOTf (0.5 mmol; **1 a**/DBU = 1 : 10000; **1 a**/LiOTf = 1 : 1000) gave quantitative yields of formate after 24 h of reaction with TON = 10000. The system was further optimized raising the temperature to 100 °C. After 24 h, with **1 a**/DBU = 1 : 50000, **1 a**/LiOTf = 1 : 5000 ratios, a TON of 31600 (63 % yield) was finally obtained (Table 1, entry 1).

The reaction mechanism involving **1 a** was then elucidated using NMR spectroscopy and DFT calculations, that showed that two interconnected mechanisms can equally contribute to the overall catalytic reaction. In the first one (Scheme 2, left), the reaction pathway involves a purely metal-centred mechanism without participation of the N–H bond of the PNP ligand. This path starts with nucleophilic attack of the hydride present in **1 a** to CO_2 in an outer sphere way, to give the intermediate complex [$Mn\{\kappa^1$-*H*-(OCHO)$\}(PNP^H$-*i*Pr)$(CO)_2$] (**1 c**) with a barrier of 9.6 kcal mol^{-1}. From **1 c**, the pathway may proceed either by formato ligand isomerisation to give [$Mn\{\kappa^1$-*O*-(OCHO)$\}(PNP^H$-*i*Pr)$(CO)_2$] (**1 d**) via a transition state with energy of 13.2 kcal mol^{-1}, or by exchange of the formate in **1 c** with a

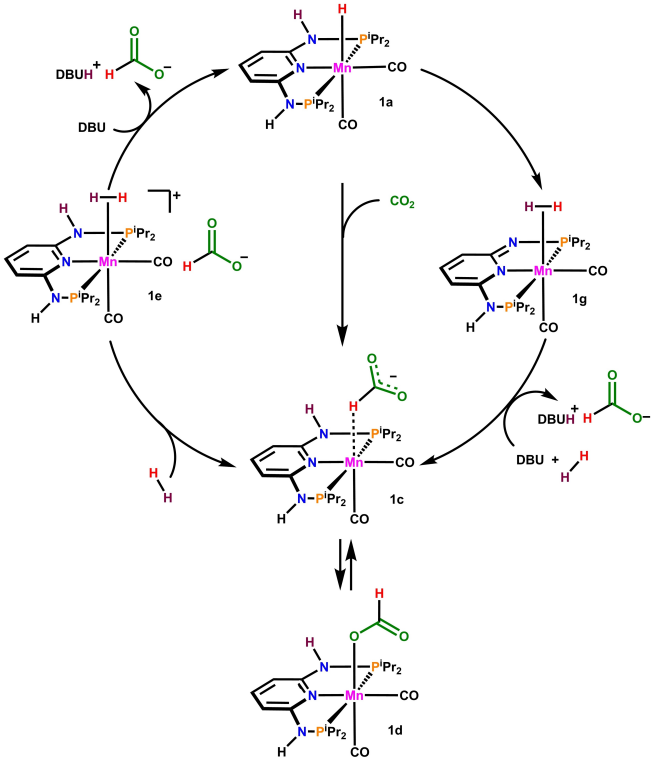

Scheme 2. Simplified, interconnected catalytic cycles for CO_2 hydrogenation in the presence of **1 a** and DBU. Reproduced (adapted) from Ref. [12].

H_2 molecule to give [$Mn(\eta^2$-$H_2)(PNP^H$-*i*Pr)$(CO)_2$] (**1 e**), that is only 7.0 kcal mol^{-1} higher in energy than **1 a** + **CO_2**. This step corresponds to the highest energy transition state of the pathway ($\Delta G^{\neq} = 17.9$ kcal mol^{-1}). Next, η^2-H_2 ligand deprotonation by either free formate or DBU base gives back **1 a** and the desired product (DBUH)(HCO_2). The overall pathway has a maximum barrier of 27.6 kcal mol^{-1}, and is thermodynamically favorable with a free energy $\Delta G = -11.2$ kcal mol^{-1}.

In the second pathway (Scheme 2, right), a bifunctional mechanism with participation of the N–H bond of the PNP ligand is active. The first step is in common with the previous one, leading to **1 c**. Next, DBU deprotonates the acidic N–H group of the PNP ligand, releasing the formate ligand as (DBUH)(HCO_2). The five-coordinate Mn neutral complex [Mn-(PNP^--*i*Pr)$(CO)_2$] (**1 f**, PNP^- = monodeprotonated PNP) coordinates H_2 to yield the intermediate [$Mn(PNP^-$-*i*Pr)$(\eta^2$-$H_2)(CO)_2$] (**1 g**), 4.2 kcal mol^{-1} more stable than **1 a** + **CO_2** in the calculations. The final step involves solvent-assisted H–H bond deprotonation from **1 f** and ligand protonation, yielding back the initial **1 a**. This step has the highest energy barrier of this pathway, at 20.0 6 kcal mol^{-1}. The overall barrier for the entire second pathway was calculated as 29.7 kcal mol^{-1}, ca. 2 kcal mol^{-1} higher than that of the first pathway, *i.e.* in reach under experimental conditions. Indeed, this observation is in line with the results of the catalytic runs, showing that **1 a** (bearing a NH bond in the ligand scaffold) is more active than **1 b**, that has instead a N–Me moiety and it is thus unable to activate a metal-ligand cooperation (MLC) mechanism.

Another interesting observation from the DFT calculations is that in the two pathways the base (DBU) has different roles. In the first case, DBU can either react with HCOOH produced from CO_2 hydrogenation yielding (DBUH)(HCO_2) in an acid-base process, or directly deprotonate the η^2-H_2 coordinated ligand. In the second mechanism, DBU deprotonates the N–H bond in the PNP ligand and forms (DBUH)(HCO_2) with the free formate anion. Finally, it was established that the LiOTf Lewis acid co-catalyst has the effect to stabilize the κ^1-*H*-coordinated formate over the κ^1-*O*-coordinated formate, that represents a thermodynamic sink common to both mechanisms, by decreasing the free energy difference between the two isomes by ca. 3.4 kcal mol^{-1}.

Almost at the same time of the report described above, Nervi, Khusnutdinova and coworkers disclosed the use of P-free, Mn(I)-complexes for CO_2 hydrogenation to formate.[13] The authors elaborated on the concept of use of Mn bipy-type proposed earlier by Pathak and coworkers,[11] synthesizing and testing a series of Mn(I) tricarbonyl complexes [MnBr(R^1R^2-bipy)($CO)_3$] (**2a–e**) and [Mn(MeCN)(R^1R^2-bipy)($CO)_3$] OTf (**3a–c**), bearing differently 4,4′- and 6,6′-substituted bipy-type ligands (R^1 or R^2 = H, OH, OMe, NH_2) shown in Figure 1. In particular, the choice of *o*-OH bis-substituted bipyridine as a ligand was inspired by natural enzymes, *i.e.* the ortho-hydroxypyridine structural fragment present in [Fe]-hydrogenase. The main purpose of the synthetic modifications was to test whether the presence of proton-shuttling groups in proximity of the metal center could help one of the crucial steps in the catalytic cycle, *i.e.* heterolytic hydrogen activation. The best results were obtained with the *o*-OH substituted complexes **2a** and **3a**, whereas only traces or moderate yields of formate were observed with the unsubstituted or *p*-substituted bipy-type complexes. Solvent screening showed that in 1,4-dioxane, with DBU as a base, 60 bar of H_2/CO_2 (1:1), 80 °C, 24 h, 97% yield of formate salt was obtained with **2a** (TON = 1224). Using CH_3CN, similar results were obtained at 65 °C using 5 μmol of **2a** (TON = 1313, 96% yield) and **3a** (TON = 1299, yield = 99%). The catalytic system involving **2a** was then optimized, by decreasing the catalyst amount to 1 μmol and running the tests at 65 °C in CH_3CN, reaching TON = 6250, 98% yield. As another example of CO_2 utilization process (amine formylation), in the same study **2a** was tested as catalyst in the presence of diethylamine and 70 bar of CO_2/H_2 (2:5) in 1,4-dioxane, and diethylformate was obtained with a TON of ca. 588 after 24 h at 80 °C.

The catalytic mechanism of CO_2 hydrogenation with this class of complexes was then studied by DFT calculations in 2018 by Das and Pati.[14] In keeping with the earlier work by Pathak and coworkers,[11] the authors confirmed that also for substituted bipy-Mn complexes the key steps are base-assisted heterolytic dihydrogen cleavage and hydride transfer to CO_2, and that both OH groups are deprotonated in the presence of DBU, as experimentally demonstrated.[13] Interestingly, it was observed that the role of the pendant oxygen atoms in ortho position is not, as it was reasonable to expect, to promote dihydrogen activation, but rather to help in reaching the correct geometry making the final hydride transfer step more feasible. In detail, it was observed that the pendant oxygen and the H_2 molecule occupy equatorial and axial sites in the active species, in turn causing geometric distortions during the water-mediated, base-free H_2 activation step. This distortion is strongly reduced by isomerization, causing these two ligands to lie in proximity on the same equatorial plane, thus giving the correct geometry for energetically more accessible H_2 activation. A simplified mechanism is shown in Scheme 3.

The use of Mn-PNN pincer-type complexes was tested by Milstein and coworkers in 2019.[15] The pincer ligands were designed in such a way to allow for metal-ligand cooperation (MLC) in substrate activation. Complexes [Mn(PNN^{tBu})($CO)_2$] (**4a**) and [Mn(PNN^{NEt2})($CO)_2$] (**4b**), obtained by treatment of the parent bromide compounds with K^{t}OBu, differ by the number and type of substituents on the amino group (one ^{t}Bu, deprotonated secondary amine *vs.* two Et groups, tertiary amine), respectively (Figure 1). Additionally, the pyridine ring in **4b** is dearomatized, with a corresponding C=C double bond on the methylene group in ortho position to the pyridine nitrogen atom. Interestingly, the study demonstrated that the activation of CO_2 follows different modes of metal-ligand cooperation, namely an amido/amino mode by [1,2]-activation of CO_2 for **4a** and a dearomatization/aromatization mode that involves [1,3]-activation of CO_2 for **4b**. This was established by testing the reactivity of the complexes with CO_2 and H_2 in separate NMR experiments. When **4a** is treated with H_2, a mixture of **4c(syn)** and **4c(anti)** was observed to form. Exposure of **4c(syn)** to CO_2 (4 bar) gave a mixture of [1,2]-CO_2 addition product (**4d**) and κ^1-*O*-formate (**4e**). Complex **4d** was also observed as unique product of the reaction of **4a** with CO_2 (1 atm), as shown in Scheme 4a. In the case of **4b**, the reaction with H_2 gave as expected the hydrido complex **4f**, upon MLC-type heterolytic dihydrogen activation and pyridine ring re-aromatization. Reaction of **4f** with CO_2 gave the κ^1-*O*-formate **4g**, whereas the reaction of CO_2 with **4b** gave instead the [1,3]-CO_2 addition product **4h** (Scheme 4b). Complexes **4a** and **4b** were tested for CO_2 catalytic hydrogenation, using 10 mol% of catalyst, KOH as base, THF, 60 bar H_2/CO_2 (1:1). After 60 h of reaction at 110 °C,

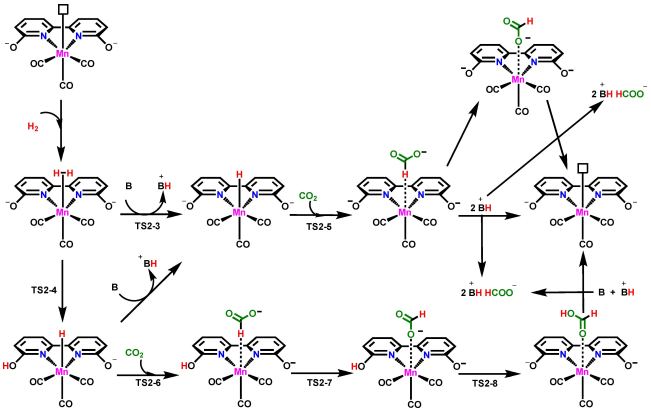

Scheme 3. Calculated mechanism for CO_2 hydrogenation to formate in the presence of **2a**. Reproduced from Ref. [14] with permission from the Royal Society of Chemistry.

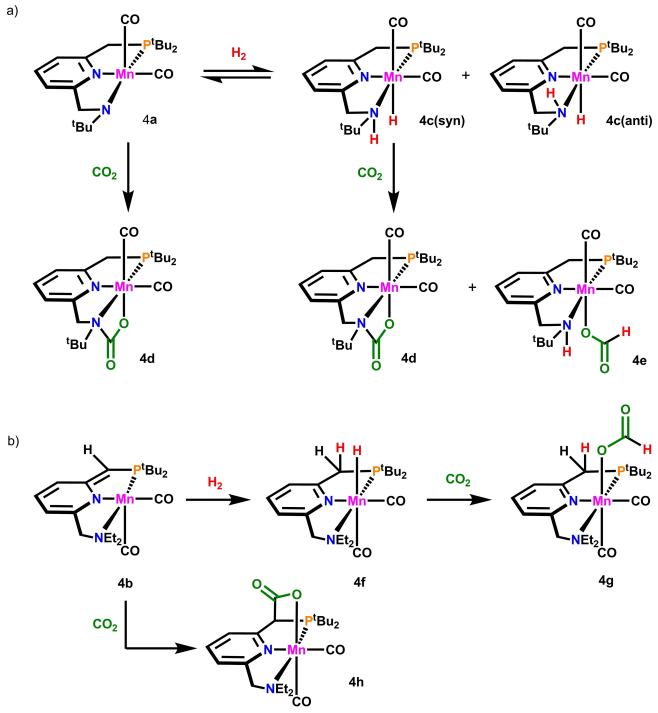

Scheme 4. Reactivity pathways of complexes **4a** and **4b** with CO_2 and H_2. Reproduced from Ref. [15] with permission from the Royal Society of Chemistry.

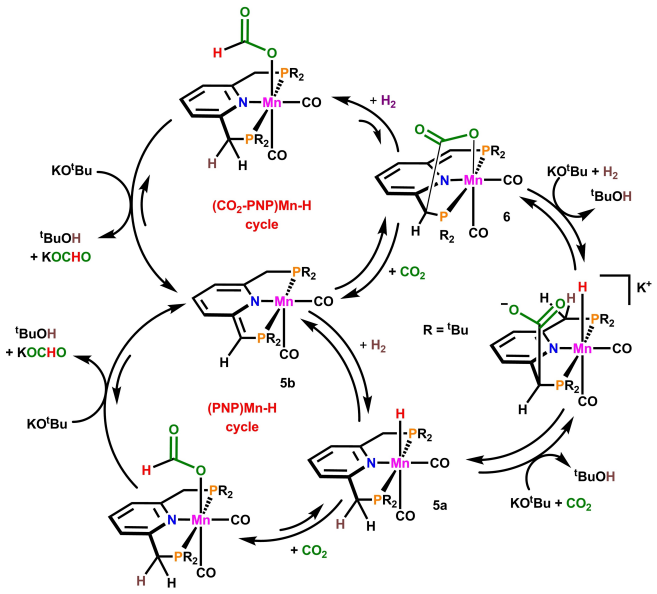

Scheme 5. Proposed mechanism and interconnected catalytic cycles starting from **5a**. Reprinted (adapted) with permission from [16]. Copyright 2021 American Chemical Society.

HCO_2K was observed in 23% and 6% yields in the case of **4a** and **4b**, respectively.

In 2021, Saouma and coworkers tested the reactivity of the PNP pincer complex [MnH(PNP^{tBu})(CO)$_2$] (**5a**, PNP^{tBu} = 2,6-bis(di-tert-butylphosphinomethyl)pyridine) for CO_2 hydrogenation.[16] As in the case of Milstein's PNN systems described above, also for complex **5a** an unexpected addition of CO_2 to the ligand backbone was observed. Detailed mechanistic and thermochemical studies showed that the Mn–H bond in **5a** is not sufficiently hydridic to reduce CO_2. Deprotonation of **5a** generates as expected complex [MnH(PNP$^-$)(CO)$_2$] (**5b**, PNP$^-$ = monodeprotonated 2,6-bis(di-tert-butylphosphinomethyl) pyridine). For **5b**, the M–H bond hydricity was calculated to be enhanced by ca. 17 kcal mol^{-1} compared to **5a**, but in spite of the sufficient hydricity to promote CO_2 hydrogenation, also in this case this reactivity was not observed. Instead, CO_2 preferentially binds to the ligand backbone in a [1,3]-fashion to generate the anionic hydride complex [MnH(PNP-CO_2)(CO)$_2$] (**6**), that was isolated by reaction of **5b** with CO_2 (0.85 bar). Complexes **5a** and **6** (5 μmol) were tested as catalyst for CO_2 hydrogenation using KO^{t}Bu (100 equiv.) as base, THF, 18 h. After a screening of CO_2/H_2 pressure and temperature, best TON = 58 and TON = 49 were obtained for **5a** and **6**, respectively, using a pressure of 30 bar (1:1 gas ratio) and 100 °C. A detailed study of stoichiometric reactivity and thermodynamic stability led to the proposal of the catalytic mechanism shown in Scheme 5, with two interconnected cycles centered on complex **5b**, leading to the formation of the active species that promote HCO_2K release.

In applied catalysis, it is often desirable to use simple, bench stable, commercially available ligands, to avoid the need for costly and time-consuming prior synthetic procedures. For this purpose, in 2021 Gonsalvi, Kirchner and coworkers studied the catalytic properties of a series of textbook Mn(I) alkylcarbonyl complexes in CO_2 hydrogenation to formate (Scheme 6).[17]

In previous studies, it was observed that complex [Mn-(^{n}Pr)(dippe)(CO)$_3$] (**7**, dippe = 1,2-bis(diisopropylphosphino) ethane) can act as long shelf-lived precursor for the catalytically active 14-electrons species [MnH(dippe)(CO)$_2$] (**7a**), that is formed *in situ* from **7** under a pressure of H_2 and elimination of butanal. Complex **7** was tested under mild reaction conditions (DBU, 40–60 bar pressure, 80 °C) for the hydrogenation of CO_2 using 1:1 to 1:3 CO_2/H_2 ratios. In the absence of additives, it was possible to obtain (DBUH)(HCO_2) with TON = 1077 after 24 h under 60 bar CO_2/H_2 = 1:1, albeit with low yields (21%). The catalytic system was substantially improved by addition of LiOTf as Lewis acid co-catalyst and by changing the gas ratio to CO_2/H_2 = 1:2 (total pressure = 75 bar). In this case a maximum TON = 1988 (yield > 98%) was obtained after 24 h, 80 °C. The mechanism was then studied by DFT calculations, showing that in the initial step, in the presence of CO_2 and H_2, pre-catalyst **7** is converted into *cis*-[MnH(dippe)(CO)$_2$(κ^1-*O*-CO_2)] (**7b**) featuring an unusual, almost linear coordination of CO_2 to Mn by one oxygen atom. The system then evolves by migratory insertion of CO_2 into the Mn–H bond, to give at first a κ^2-*CH,O*-formato complex **7c** featuring an agostic interaction with a long C···H separation (3.27 Å), that in turn gives the coordinatively unsaturated complex *cis*-[Mn(κ^1-*O*-OCOH)(dippe)(CO)$_2$] (**7d**), more stable than **7c** by 5 kcal mol^{-1}. Complex **7c** is stabilized by chelation giving [Mn(κ^2-*O,O*-OCOH)(dippe)(CO)$_2$] (**7e**), that can be considered the resting state of the catalyst in absence of CO_2/H_2 pressure. Upon H_2 coordination to the metal center, the

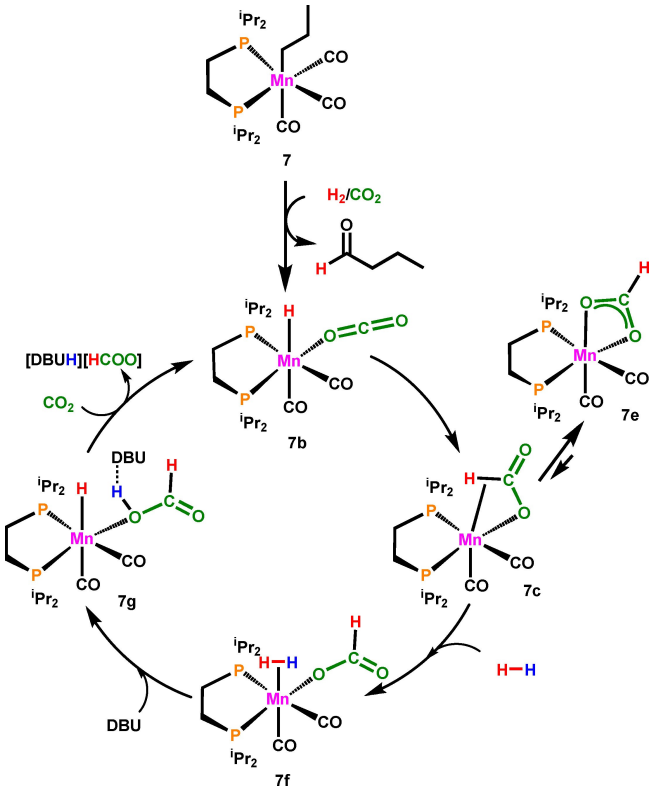

Scheme 6. Simplified mechanism for CO_2 hydrogenation to formate with **7**. Reproduced (adapted) from Ref. [17].

catalytic cycle proceeds from **7e** to *cis*-[Mn(η²-H_2)(κ¹-*O*-OCOH)(dippe)$(CO)_2$] (**7f**). The dihydrogen ligand is then activated by the base (DBU), giving a formate complex **7g**, H-bonded to the protonated base ($DBUH^+$). Formate is finally released to regenerate the active species **7b** in the presence of CO_2 (Scheme 6).

The importance of metal-ligand cooperation in Mn-catalyzed CO_2 hydrogenation has been studied by many authors, and in particular the beneficial effect of the presence of a free N atom in the ligand backbone, able to participate in substrate activation, has been evaluated and described both by experimental and computational means. In 2017, a predictive DFT calculations study by Yang and coworkers[18] examined the potential of a series of manganese and cobalt complexes of the type $[M(^{tBu}P_2{}^{tBu}N_2)(R_1)(R_2)(R_3)]$ (M=Mn, R_1=R_2=CO; M=Co, R_1=R_2=CN; R_3=H, CN, NO_2, CH_3, NH_2, OH, CHO, COOH, $COCH_3$, and $COOCH_3$) as catalysts for the direct hydrogenation of CO_2 to methanol. These complexes, extensively studied by Bullock, DuBois and coworkers in particular for dihydrogen activation,[19] feature a multidentate PNNP ligand with a pendant amine arm, having the correct basicity to facilitate dihydrogen heterolytic splitting by accepting a proton from the metal-coordinated η²-H_2 ligand. In the computational study, the calculations showed that the overall process proceeds *via* three cascade catalytic reactions, namely i) the hydrogenation of CO_2 to HCOOH, ii) the hydrogenation of HCOOH to formaldehyde (HCHO) with the formation of water, and iii) the hydrogenation of HCHO to methanol. In the case of complex [Mn(κ¹-*O*-OCHO)$(^{tBu}P_2{}^{tBu}N_2)(CN)_2$] (Scheme 7), a rather accessible overall energy barrier (27.7 kcal mol^{-1}) was calculated. The key difference for the Mn-based system compared to the Co-based analogue is that instead of the step-by-step release of CH_2O and transfer of the proton on N to the hydroxyl for the formation of H_2O for Co, in the case of Mn the release of CH_2O and transfer of the proton on N1 to the hydroxyl group to give H_2O is a simultaneous process from a single transition state. In turn, this implies that the hydrogenation of HCHO to CH_3OH is fast and with a low energy barrier (12.7 kcal mol^{-1}).

Among PNP pincer-type ligands, the bis-(phospino)amine $[HN(C_2H_4P^iPr_2)_2]$, commonly denoted ^{i}Pr-MACHO, has often been used by many research groups worldwide to obtain the corresponding precious and earth-abundant metal complexes.

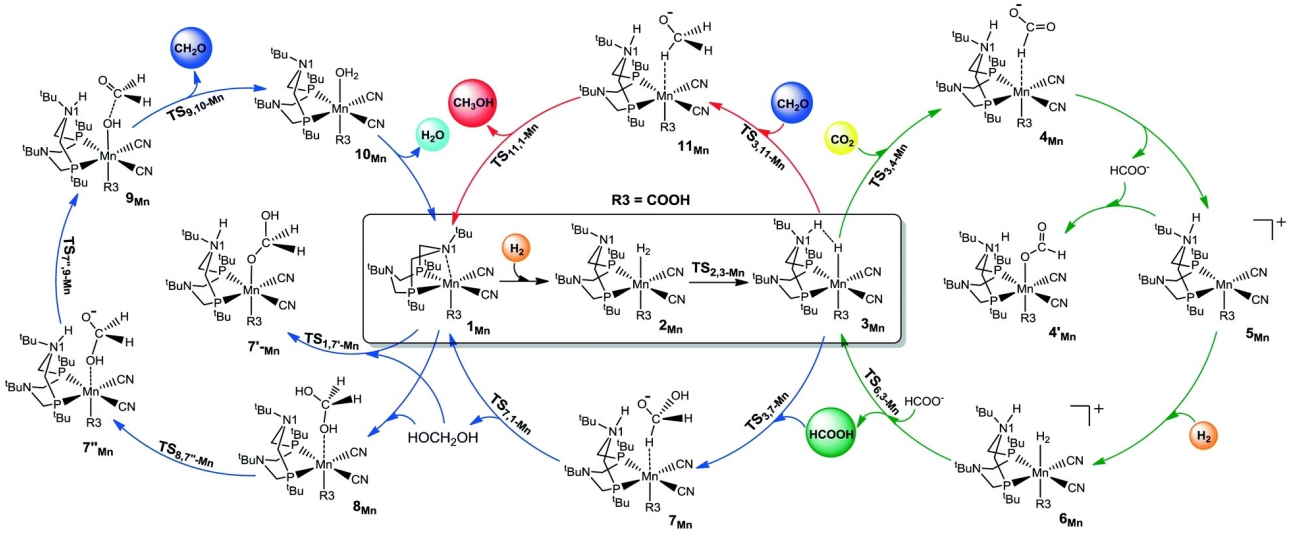

Scheme 7. The calculated catalytic mechanism for the conversion of CO_2 to CH_3OH in the presence of [Mn(κ¹-*O*-OCHO)$(^{tBu}P_2{}^{tBu}N_2)(CN)_2$]. Reproduced from Ref. [18] with permission from the Royal Society of Chemistry.

This simple aminophospine ligand often brings about metal-ligand cooperation by reversible protonation/deprotonation at the nitrogen atom, in such a way that amino/amido species are involved in the catalytic processes. In 2021, Leitner and coworkers applied the amido complexes $[Mn\{N(C_2H_4PR_2)_2\}(CO)_2]$ (R = ^{i}Pr, **8a**; Ph, **8b**; ^{t}Bu = **8c**) as catalysts for the direct hydrogenation of CO_2 to MeOH, in the presence of Lewis acids such as $Sc(OTf)_3$ and $Ti(O^iPr)_4$ and a mixture 1,4-dioxane/EtOH as solvent.[20]

Control experiments showed that the role of the Lewis acid is to act as an esterification promoter to remove the formate ligand from the Mn coordination sphere of the Mn-formato complexes, that otherwise represent the resting state of the catalysts. Under optimized conditions, i.e. H_2/CO_2 ratio > 30, 150 °C, 68 h, $Ti(O^iPr)_4$, a TON_{max} = 87 was obtained in the presence of **8b** (Table 1). Mechanistic details were obtained in 2022 by the same authors, by a combination of experimental and computational data.[21] Quantum chemical computations at the density functional theory and DLPNOCCSD(T) level of theory confirm the previous hypothesis of a formate resting state as the most stable intermediate. Using CH_3OH as solvent in the calculations, in the presence of **8a** the reaction sequence considered involves i) CO_2 hydrogenation to HCOOH, ii) methanol esterification to methyl formate, iii) methyl formate hydrogenation, iv) hemiacetal decomposition to give free HCHO and v) HCHO hydrogenation to methanol (Scheme 8).

The initial Mn–H active species is obtained by a Dub-type mechanism involving proton shuttle-assisted activation of dihydrogen, centered on the activated Mn complex, by the alcohol solvent. Next, CO_2 inserts into the Mn–H bond to give the Mn-formato species by hydride transfer without the need for pre-coordination. The Lewis acid then promotes the esterification of HCOOH to formate ester. Next, hydride transfer to the formate ester gives a hemiacetal anion that decomposes to HCHO by cleavage of its C–O bond. The following hydrogenation of formaldehyde has a very low barrier and proceeds by a concerted hydride and proton transfer to the carbonyl carbon. The rate-determining states (RDSs) of the reaction belong to the hydrogenation of a formate ester to methanol step, as determined by DFT calculations and experimental concentration−time profiles. The rate-determining step was finally confirmed to be hydrogen splitting, by measuring kinetic isotope effects (KIE) using H_2/D_2 and EtOH/EtOD mixtures.

It is interesting to observe that, at a predictive DFT calculation level, even small changes in the ligand architecture can have a profound influence on the overall reaction mechanism. In 2021 Lei and coworkers used a density functional theory (DFT) calculations approach to explore the reaction mechanism of the three cascade cycles for the hydrogenation of carbon dioxide to methanol catalyzed by the manganese PNP pincer complex $[Mn\{(Ph_2PCH_2SiMe_2)_2N\}(CO)_2]$, that differs only slightly from the MACHO-type ligands, by the presence of $SiMe_2$ moieties in place of a methylene group of the backbone.[22] This complex was previously experimentally used as efficient catalyst for hydroboration reactions, including the conversion of CO_2 to methoxyborane, by Leitner and coworkers in 2018 (see Section 3).[23] In the case of CO_2 hydrogenation to methanol, the study showed a remarkable solvent effect changing the RDS. Under solvent-free conditions, the calculations showed that hydrogen activation is the rate-determining step of each of the three catalytic cycles, namely CO_2 hydrogenation to HCOOH, formic acid reduction to HCHO and hydrogenation of formaldehyde to methanol, with an overall highest barrier of 27.1 kcal mol^{-1}. By introducing different solvents such as water, toluene and THF in the calculations, the RDS of this reaction corresponds to the hydrogen transfer step of the formic acid hydrogenation stage, with energy spans of 21.3, 20.8 and 20.4 kcal mol^{-1} for the three solvents, respectively. The initial Mn–H species is generated as expected by MLC-type heterolytic dihydrogen splitting accompanied by ligand protonation at the N atom. The N–H moiety then also assists in the outer-sphere hydrogenation of formic acid to methanediol and the decomposition of methanediol to formaldehyde (Figure 2).

Within the family of Mn-MACHO complexes, N-protonated analogues of **8**, namely complexes $[MnBr\{NH(C_2H_4PR_2)_2\}(CO)_2]$ (R = ^{i}Pr, **9a**; Cy, **9b**; Ph, **9c**; ^{t}Bu = **9d**) were used in 2022 by Sponholz, Junge, Beller and coworkers as pre-catalysts for the reversible CO_2 hydrogenation to formate and HCOOH selective dehydrogenation to ($H_2 + CO_2$) gas mixtures. Another type of pincer type catalysts used in the study are complexes $[MnBr(PN^5P)(CO)_2]$ (**10a–c**, Figure 1). The PN^5P ligands are based on 2,6-bis(diisopropylphosphineamino)triazines bearing different R substituents in 4-position (R=Me, **10a**; R=NH(C_3H_5), **10b**; R = $(CH_2)_2$-1-imidazoyl, **10c**).[24] The catalytic protocol, based on the use of aminoacids such as lysine (Lys) and the corresponding potassium lysinate (LysK) salt, represents a sustainable hydrogen storage and release method, bringing together reversible hydrogenation of CO_2 to HCOOH and carbon capture processes. Under standard reaction conditions, *i.e.* Lys (5.0 mmol), Mn catalyst (0.02 or 0.10 μmol), H_2O/THF (1:1, 10 mL total), CO_2/H_2 (1:3, 80 bar total), 85–145 °C, 12 h, the best results were obtained with **9a** (TON = 40000, 145 °C) and **10b** (TON = 230000), the latter representing the current state-of-the-art TON for Mn-catalyzed CO_2 hydrogenation to formate to date. Complex **10b** also resulted to be a very efficient catalyst for H_2 evolution from formic acid (5.0 mmol) in the presence of Lys (1.0 equivalent) at 90 °C, 12 h, reaching TON = 29400 and > 99% HCOOH conversion. By recharging the reaction vessel, up to 10 consecutive runs were possible for CO_2 hydrogenation, leading to a total TON (TTON) of ca. 2000000. To avoid the drawback of CO_2 recharging in consecutive runs, and with the aim of providing a practical system for a chemical hydrogen battery, the use of LysK in place of Lys was tested, as this salt is known for its property to capture CO_2. After one cycle of hydrogen release and storage, formate (92%) was obtained

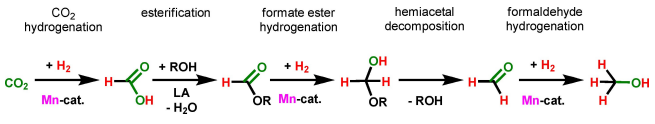

Scheme 8. Stepwise reaction pathway for CO_2 hydrogenation to CH_3OH in the presence of **8a**. Reproduced (adapted) from Ref. [21].

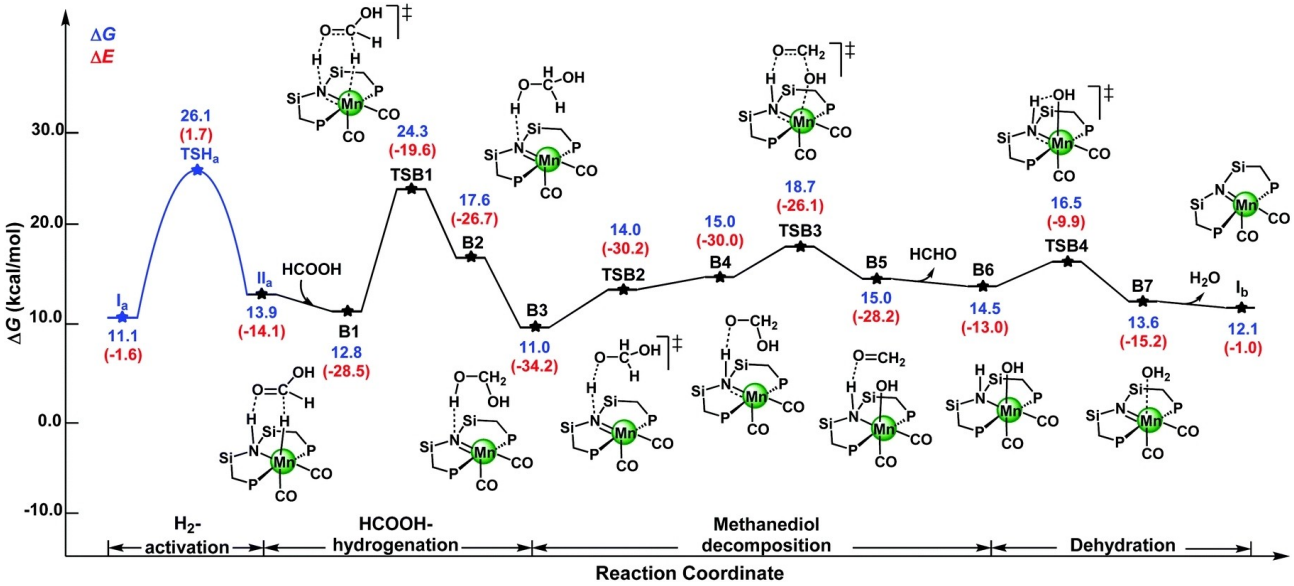

Figure 2. Calculated reaction pathway of the hydrogenation of HCOOH to methanediol and the decomposition of methanediol to HCHO and water catalyzed by complex [Mn{$(Ph_2PCH_2SiMe_2)_2NH$}$(CO)_2$]. Reproduced from Ref. [22] with permission from the Royal Society of Chemistry.

applying 5 mmol LysK. In a scaled-up prototype, the H_2 evolution process applying LysK was carried out without drop of the efficiency in at least ten charge–discharge cycles, without the need to feed CO_2 to the reactor after the first run. Mechanistic details were obtained by NMR experiments, that allowed the authors to propose a catalytic cycle for reversible CO_2 hydrogenation in the presence of pre-catalyst **10b** (Scheme 9).

The first step involves pre-catalyst activation by LysK via N–H deprotonation and dearomatisation of the triazine moiety, giving a bimetallic Mn–K active species. Then, in the CO_2 hydrogenation pathway (H_2 storage), dihydrogen is activated via heterolytic cleavage to give the corresponding Mn-hydrido complex, with protonation of LysK to Lys. CO_2 insertion into the Mn–H bond follows to give the Mn-formato species. Finally, HCOOH is liberated by converting 1 equivalent of Lys to LysK, regenerating the active Mn species after dearomatisation of the triazine moiety.

Other reaction pathways and mechanisms involving Mn-MACHO pincer complexes were evaluated. Base-free CO_2 hydrogenation to formate in the presence of **8a** was studied by DFT calculations by Rawat and Pathak in 2017, focusing in particular on the role of substituents on the P donor atoms.[25] The calculated catalytic cycle (Scheme 10) starts from H_2 coordination to **8a** to give a Mn(η^2-H_2) complex bearing deprotonated PNP ligand. Then, by MLC-type heterolytic H_2 cleavage, a Mn–H species with protonated PNP is formed. The hydrido complex then undergoes CO_2 insertion into the Mn–H bond to give a κ^1-*H*-formato complex. HCOOH is formed by proton transfer from the ligand N atom to the O^-atom of thecarboxylic group, and it is then released to regenerate **8a**. The calculations showed that heterolytic H_2 cleavage (RDS) is favored by strong π-acceptor

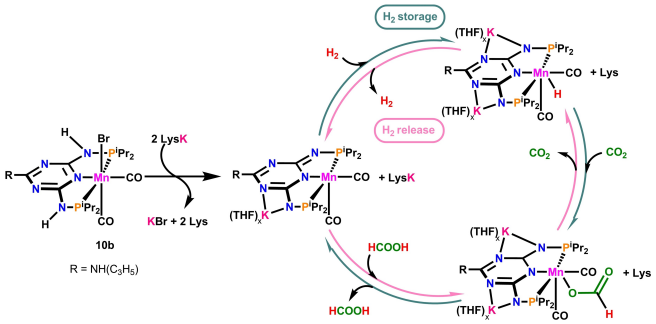

Scheme 9. Proposed catalytic cycles for hydrogen storage and release by reversible CO_2 hydrogenation and HCOOH dehydrogenation in the presence of **10b**. Reproduced (adapted) from Ref. [24].

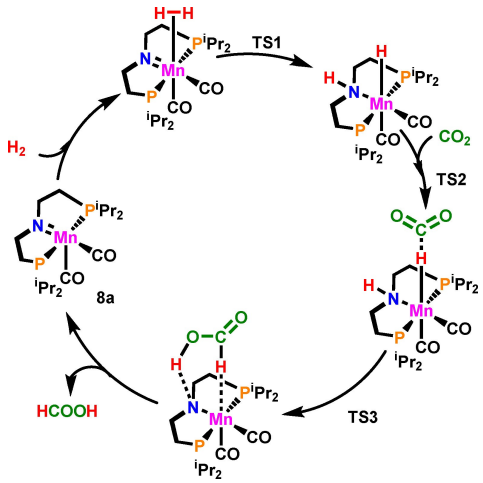

Scheme 10. DFT calculated catalytic mechanism for the base-free hydrogenation of CO_2 to HCOOH in the presence of **8a**. Reproduced from Ref. [25] with permission from the Royal Society of Chemistry.

ligands and hydride transfer is favoured by strong σ-donor ligands.

In 2022, Bersnkoetter, Hazari and coworkers experimentally applied complexes analogues of **9a**, namely $[MnR^2\{NR^1(C_2H_4P^iPr_2)_2\}(CO)_2]$ ($R^1=H$, $R^2=H$, **11a**; $R^1=Me$, $R^2=H$, **11b**; $R^1=H$, $R^2=OC(O)H$, **11c**; $R^1=Me$, $R^2=OC(O)H$, **11d**), for CO_2 hydrogenation to formate in the presence of base (DBU) and LiOTf as Lewis acid co-catalyst.[26] The two MACHO-type ligands used in this study present different substituents on the N atom, either $R^1=H$ (secondary amine) or $R^1=Me$ (tertiary amine), and only the former can in principle bring about a MLC-type catalytic mechanism by amino/amido reversible deprotonation involving **8a** as intermediate. Catalytic data (Table 1) show that the hydrido complex **11b**, bearing $R^1=Me$, outperforms the other analogues reaching TON = 18300, 73% yield after 24 h, 80 °C, CO_2/H_2 (1:1, 68 bar total pressure). These results demonstrate that MLC-type mechanisms do not necessarily lead to better catalyst performances. The authors carried out mechanistic experiments showing that CO_2 insertion into the M–H bond of each catalyst affords stable manganese formate complexes, and these are intermediates in the catalytic cycles as confirmed by *in situ* NMR measurements.

The authors concluded that the tertiary amine-based system gives better catalytic performance due to a combination of longer catalyst lifetime and greater enhancement from LiOTf co-catalyst. The proposed catalytic cycles for **11a** and **11b** are shown in Scheme 11.

As shown above, the Mn(I) pincer complexes used as catalysts for CO_2 hydrogenation feature a stabilizing PNP ligand forcing meridional coordination to the metal, two CO ligands and either a vacant site (pentacoordinate Mn geometry) or a bromide/hydride ligand in apical position. In 2023, Gonsalvi and coworkers showed that even tris(carbonyl), halide-free, coordinatively saturated neutral Mn(I) pincer complexes can bring about CO_2 hydrogenation.[27]

Complex $[Mn(PNP)(CO)_3]$ (**12a**, PNP = deprotonated bis(2-(diisopropylphosphino)-4-methylphenyl)amine) was tested under various conditions of pressure, temperature, catalyst/DBU ratio, in the presence and in absence of LiOTf co-catalyst. Under optimized conditions, *i.e.* 0.02 mol% of catalyst, DBU/LiOTf = 10:1, THF, 5.5 mL; 60 bar total pressure H_2/CO_2 (1:1); 80 °C; 72 h, a maximum TON = 3805 was obtained, with 76% formate yield. DFT calculations showed that **12a** can be converted into the putative pentacoordinate $[Mn(PNP)(CO)_2]$ (**12b**) active species under catalytic conditions, a step that requires 16.3 kcal mol^{-1}. The anionic hydrido complex $[MnH(PNP)(CO)_2]^-$ (**12c**) is then formed by DBU-assisted intermolecular dihydrogen heterolytic cleavage, instead of an intramolecular MLC-type mechanism assisted by the N donor atom of the PNP ligand. A possible explanation of such an unexpected mechanism is the higher Lewis basicity of the DBU nitrogen atom compared to that of the amido group of the ligand. The protonated base $(DBUH)^+$ then helps in final step, the release of coordinated formate from the metal coordination sphere. The overall highest barrier of the entire catalytic cycle (Scheme 12) was calculated as *ca.* 20 kcal mol^{-1}, that is well reachable under the experimental reaction conditions.

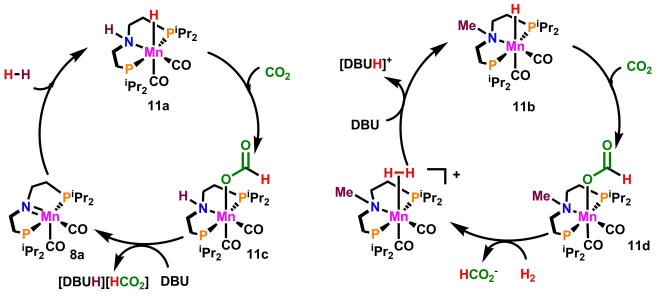

Scheme 11. Simplified mechanisms for CO_2 hydrogenation to formate with **11a** and **11b**, respectively. Reprinted (adapted) with permission from [26]. Copyright 2022 American Chemical Society.

2.2. Indirect hydrogenation

Only three reports on Mn-catalyzed, amine-mediated indirect CO_2 hydrogenation to CH_3OH have appeared in the literature. In 2017, Prakash and coworkers applied complex **9a** as pre-catalyst for the two-step CO_2 reduction to CH_3OH, in the presence of various amines and bases (Scheme 1b).[28] The role of the amines is to react with HCOOH, formed by 2-electrons CO_2 reduction, to give the corresponding formamides. These are then hydrogenated to CH_3OH, regenerating the initial amines. In the experimental setup, the reactor was initially

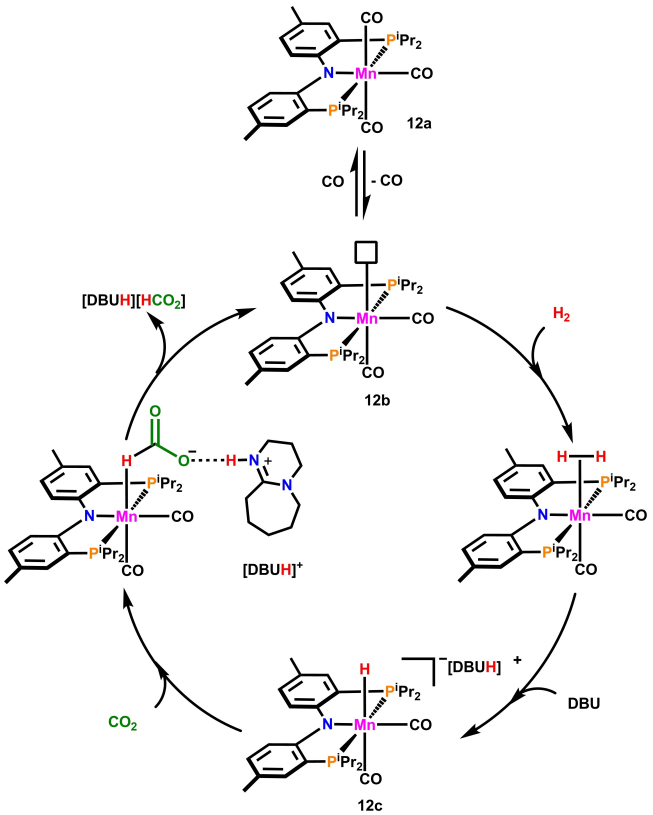

Scheme 12. Proposed mechanism for CO_2 hydrogenation to formate with **12a**. Reproduced (adapted) from Ref. [27].

charged with the catalyst, solvent, amine, base, CO_2/H_2 gas pressure and then heated to the desired temperature for the chosen time. After this time, analysis of aliquots of the reaction mixture allowed to quantify the yields in formamides. The experiments were repeated, and after the end of the formylation step the gas inside the reactor was vented, then fresh H_2 (pressure) and base were added to the reactor containing the reaction mixture and the catalyst. After heating for a set time, the crude mixtures were analyzed to evaluate the amount of methanol formed during the formamide hydrogenation step. K_3PO_4 and ^{t}BuOK were used as bases, whereas the best amines, after a due screening, were found to be morpholine, benzylamine and *N*-methylbenzylamine. For the first step, it was shown that pre-catalyst **9a** (0.5 mol%) was able to promote the formation of 4-formylmorpholine in 77% yield, using K_3PO_4 (2.5 mol%) CO_2/H_2 (1:1, 60 bar total pressure), 110 °C in THF after 24 h. Upon optimization, a maximum yield = 95% was obtained, using 2.0 mol% of catalyst and ^{t}BuOK (10 mol %), 36 h. Using pure 4-formylmorpholine as substrate, this was effectively reduced to morpholine and CH_3OH (64% yield, TON = 128) at 0.5 mol% catalyst loading in THF after 24 h under 70 bar of H_2 pressure and 150 °C in the presence of **9a**. On the other hand, in the sequential formylation-hydrogenation experiment, adding an additional 80 bar of H_2 to the mixture used for morpholine formylation under optimized conditions, running the test at 150 °C, 36 h, CH_3OH was obtained in high yield (71%) corresponding to TON = 36. Attempted one-pot reduction of CO_2 to CH_3OH using **9a**, 5 bar CO_2 and 85 bar H_2, 150 °C, 24 h in the presence of morpholine was however unsuccessful, with only 5% yield in 4-formylmorpholine. The yield in formamide was increased to 38% by a different experimental setup consisting of stepwise temperature increase, but also in this case only traces of CH_3OH were observed. The reaction mechanism was studied by NMR spectroscopy, and the experimental evidences so obtained suggest a pivotal role of the Mn-formato complex **11c** for both reactions (Scheme 13).

The reaction mechanism was further studied by DFT calculations and microkinetics in 2019 by Pathak and coworkers.[29] The amidation step, involving a metal-free organic reaction between HCOOH and morpholine, was calculated to be highly exergonic (−10.4 kcal mol^{-1}), and this helps to increase the overall rate of the reaction. It was then observed that the following *N*-formylmorpholine hydrogenation step may follow two competitive pathways with comparable free energy barriers. As shown in Scheme 14, path a) starts from the activation of *N*-formylmorpholine by **11a**, bringing about C=O bond hydrogenation, followed by C=N bond hydrogenation to give morpholine and CH_3OH with the regeneration of **11a**. The highest energy barrier for path a) was calculated as 38.2 kcal mol^{-1}. In competitive path b) instead, C=N hydrogenation occurs first, releasing morpholine, then C=O bond hydrogenation releases CH_3OH regenerating **11a**. For path b), the highest energy barrier was calculated as 38.4 kcal mol^{-1}, thus both pathways can equally contribute to the overall catalytic mechanism.

In 2023, Al Thabaiti, Lahiri, Maiti and coworkers reported on the use of a Mn-SNS pincer complex for the indirect CO_2 hydrogenation to CH_3OH.[30] The authors applied the benchstable complex [Mn(SNS)(CO)$_3$]Br [**13a**, SNS = bis(2-(ethylthio)ethyl)amine)] as pre-catalyst for the reaction in the presence of amine shuttles, including morpholine, piperidine, benzylamine, 3,4-dimethylbenzyl amine, 3-methoxybenzyl amine.

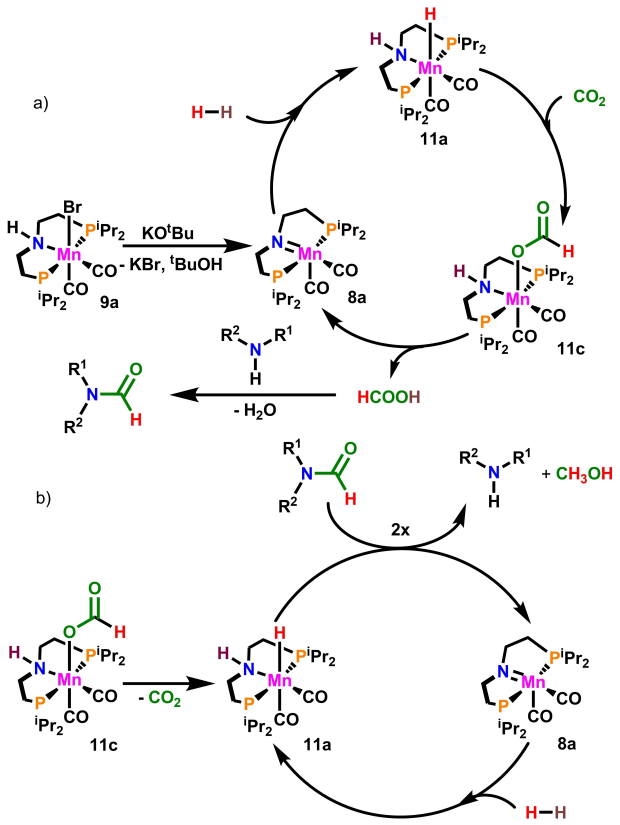

Scheme 13. Proposed mechanisms for the synthesis of formamide from CO_2 hydrogenation (a) and formamide hydrogenation to methanol (b) starting from pre-catalyst **9a**. Reprinted (adapted) with permission from [28]. Copyright 2017 American Chemical Society.

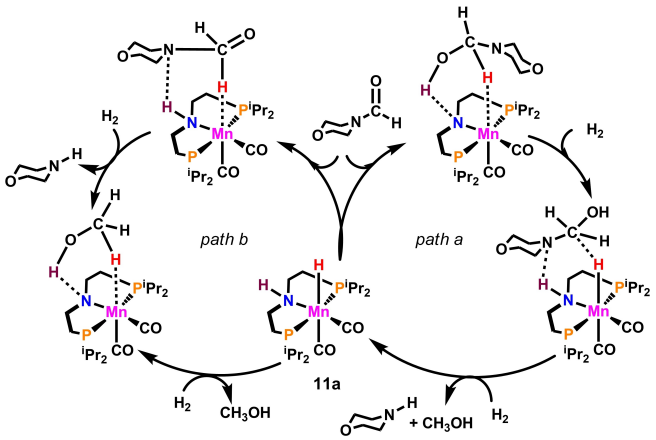

Scheme 14. Competitive pathways for *N*-formylmorpholine hydrogenation to CH_3OH catalyzed by **11a**. Reproduced from Ref. [29] with permission from the Royal Society of Chemistry.

The tests were run using THF as solvent, CO_2/H_2 (1:1, 20 bar total pressure), 1 mol% of catalyst, K_3PO_4 as base (1 to 2 equiv.), 120 °C, 24 h. Under these mild conditions, formamides were obtained in high yields, *i.e.* up to 91% for *N*-formylmorpholine, using 2 equiv. of base, however no traces of CH_3OH were observed. By changing the CO_2/H_2 ratio to 1:6 (70 bar total pressure) and heating the reaction mixture to 110–140 °C for 24 h, methanol formation was detected by GC analysis. The authors calculated a TON = 60 for methanol formation, however this value was only estimated by NMR spectroscopy, from the decrease of the signal corresponding to the –CHO group of N-formylmorpholine, and not quantified against an internal standard. The proposed catalytic mechanism (Scheme 15) involves two steps, *i.e.* amine formylation by *in situ* generated HCOOH (step i) and formamide hydrogenation to CH_3OH (step ii), both centered on the putative hydrido complex $[MnH(SNS)(CO)_2]$ (**13b**).

3. CO_2 hydroboration

Among possible alternative reductants to replace hydrogen, hydroboranes (R_2BH) have the advantage of being easier to store and handle, due to their liquid state at room tempearture and pressure. Already under mild reaction conditions, they can bring about CO_2 reduction to various products (Scheme 1c) such as formoxyborane (A), bis(boryl)acetal (B), methoxyborane (C) and bis(boryl)ether (D), due to the much weaker nature of the B–H than H–H bond, making the formation of new B–O bonds much easier. The state of the art for CO_2 hydroboration to formoxyborane (A) was obtained by Hazari and coworkers. The use of [PdH(^{Cy}PSiP)] (0.001 mol%), pinacolborane (HBpin, 0.050 mmol) and CO_2 (1 bar) in C_6D_6 leads to a very high catalytic performance with a TON of 63500 (TOF = 529 h^{-1}) obtained after 5 days of reaction at 25 °C.[31] In the case of methoxyboranes (C), the best results were obtained by Chen and coworkers using bis(phosphinite) POCOP-type Ni(II) pincer complexes of general formula [NiX{2,6-$(R_2PO)_2C_6H_3$}] (R = ^{t}Bu, X = SC_6H_4-*p*-OCH_3; R = ^{i}Pr; X = N_3). The catalytic hydroboration of CO_2 was carried out in the presence of catecholborane (HBcat) with 0.2 mol% of catalyst in C_6D_6 at room temperature to obtain TONs of 490 (TOF = 2400 h^{-1}) and 477 (TOF = 1908 h^{-1}), respectively.[32]

In the last decade, part of the chemistry community has focused on the quest for cheaper catalysts based on earth-abundant metals to increase process sustainability for CO_2 hydroboration.[33] The results of Mn-catalyzed CO_2 hydroboration are hereby summarized. Drawings of the molecular structures of the competent Mn catalysts are shown in Figure 3. Table 2 summarizes the main reaction conditions and catalytic results for all the described complexes.

The first example of use of a manganese complex in CO_2 hydroboration was described by Leitner and coworkers in 2018.[23] In the presence of complex [MnBr{$(Ph_2PCH_2SiMe_2)_2NH$}$(CO)_2$] (**14**), the selective formation of methoxyborane was obtained with high TON = 883 using pinacolborane (HBpin, 2.76 mmol), CO_2 (1 atm), catalyst (0.036 mol%), base (NaO^{t}Bu, 0.2 mol%), under solventless conditions at moderate temperatures (100 °C). The proposed stepwise reduction mechanism (Scheme 16) begins with the base-assisted activation of **14** to generate the coordinatively unsaturated active species [Mn{$(Ph_2PCH_2SiMe_2)_2N$}$(CO)_2$] (**14a**) bearing the deprotonated PNP ligand. This step has been confirmed experimentally by $^{31}P\{^1H\}$ NMR, with the observation of a signal at 61.3 ppm due to **14a**. Reaction of **14a** with HBpin leads to the activation of the B–H bond of the hydroborane by formation of a four-center coordination moiety bearing a new B–N bond and partial hydride transfer to the metal center in intermediate **14b**, characterized by a ^1H NMR signal at −6.6 ppm and a $^{31}P\{^1H\}$ NMR signal at 65.2 ppm. For **14b**, single crystal structure X-ray determination was also obtained. Mechanistic studies showed that heating a sample of **14b** in THF-d_8 caused its slow conversion to a Mn-hydride complex upon full

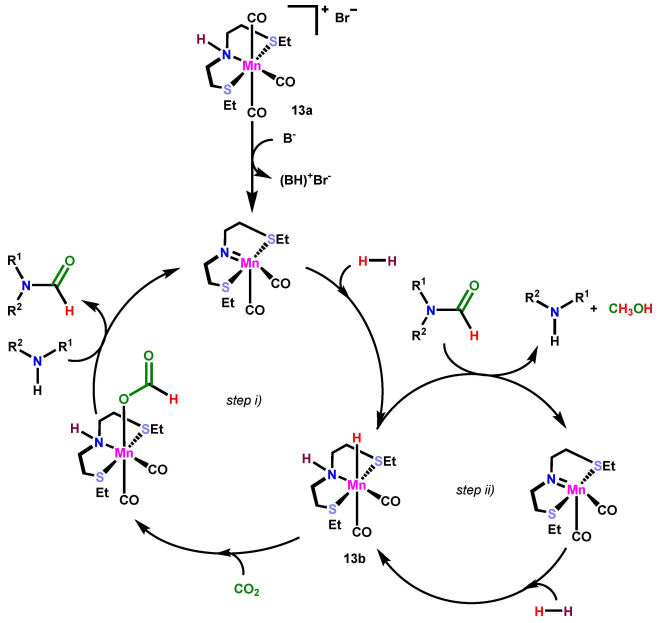

Scheme 15. Proposed stepwise CO_2 hydrogenation to CH_3OH catalyzed by **13**. Reprinted (adapted) with permission from [30]. Copyright 2023 American Chemical Society.

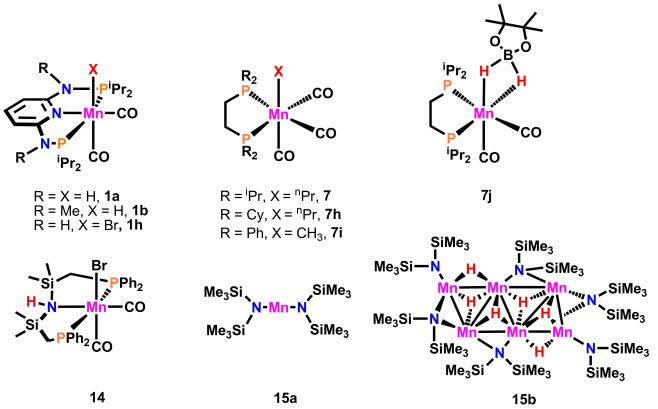

Figure 3. Chemical drawings of Mn complexes used as catalysts for homogeneous CO_2 hydroboration.

Table 2. Summary of main reaction parameters, type of products and best yields and TONs for Mn(I)-catalyzed CO_2 hydroboration.

Catalyst	Amount of cat. [mol%]	Solvent	Temp. [°C]	Time [h]	Additives	Type of product(s)[a] (type of HBR_2)	Yield [%] [b]	Best TON[c]	Ref.
14	0.072	–	100	14	NaO^{t}Bu	C, D (HBpin)	96	883	[23]
1a	1	THF-d_8	60	24	$B(OPh)_3$	C, D (HBpin)	78	26	[36]
1a	1	THF-d_8	60	5	$B(OPh)_3$	C, D (9-BBN)	74	25	[36]
1b	1	THF-d_8	60	24	$B(OPh)_3$	C, D (HBpin)	8	3	[36]
1f	1	THF-d_8	60	24	$B(OPh)_3$	C, D (HBpin)	31	10	[36]
15a	5	C_6D_6	80	72	–	C (HBpin)	21	1	[38]
15b	5	C_6D_6	80	20	–	C (HBpin)	18	1	[38]
7	1	dmso-d_6	60	24	–	C, D (HBpin)	99	33	[39]
7h	1	dmso-d_6	40	5	–	C, D (HBpin)	76	25	[39]
7i	1	dmso-d_6	60	3	–	C, D (HBpin)	12	4	[39]
7j	1	dmso-d_6	60	3	–	C, D (HBpin)	100	33	[39]

[a] Products:formoxyborane (A), bis(boryl)acetal (B), methoxyborane (C), bis(boryl)ether (D); type of hydroborane used in brackets; [b] Yield of product C; [c] TON was calculated for product C.

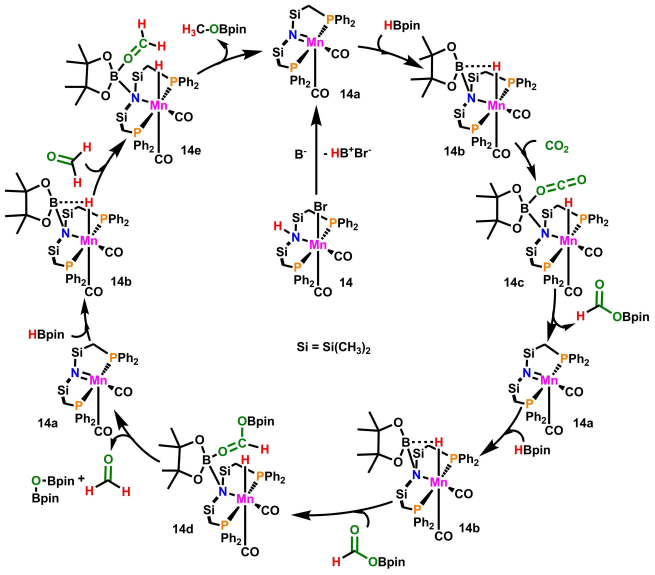

Scheme 16. Proposed catalytic cycle for CO_2 hydroboration to methoxyborane in the presence of **14**. Reproduced (adapted) from Ref. [23].

cleavage of the B–H bond and hydride transfer to Mn, identified by a ^{1}H NMR signal at −7.67 ppm and $^{31}P\{^1H\}$ NMR signal at 57.8 ppm. This species then activates carbon dioxide by formation of a B–O bond to give complex **14c**, that undergoes nucleophilic attack at the C atom of CO_2 to give the formoxyborane (OCHO)Bpin. The formoxyborane product is then released, regenerating **14a**. In the following step, a second molecule of pinacolborane reacts with **14a** to give again **14b**. Formoxyborane interacts with **14b** making a new B–O bond in **14d**. Upon hydride transfer to the C atom, reduction of the C=O bond occurs with formation of the acetal $H_2C(OBpin)_2$, that cleaves into formaldehyde and pinBOBpin releasing **14a**. Finally, after prior formation of **14b**, the reduction of HCHO occurs with release of methoxyborane $(CH_3O)Bpin$, closing the catalytic cycle.

The reaction mechanism was later studied by other authors by DFT calculations. Wan, Li and Liao in 2021 carried out calculations on the reaction pathway, to pinpoint the unsolved key issues of the mechanism proposed by Leitner and coworkers on the basis of experimental data. As in the experimental paper, the mechanism was divided in four steps, namely i) the addition of HBpin to the unsaturated Mn active species, ii) the reduction of CO_2 to (OCHO)Bpin, iii) the reduction of (OCHO)Bpin to HCHO and iv) the reduction of HCHO to $(CH_3O)Bpin$. The calculations confirmed that the common feature of all reduction steps is the ligand-assisted activation of HBpin by σ-bond insertion into the unsaturated Mn–N bond in complex **14a**, followed by nucleophilic attack of the Mn–H complex to the electrophilic carbon centers. The hydride transfer to (OCHO)Bpin was found to be the rate-limiting step for the whole catalytic cycle, with a total barrier of 27.0 kcal mol^{-1}. It was confirmed that CO_2 activation in the first step occurs by B–O coordination to give **14c**, followed by a concerted hydride transfer to give a Mn-coordinated κ^1-*H*-formato species in an almost barrierless step. Formato ligand rearrangement follows with the formation of a N–B-O bond, ending with release of (OCHO)Bpin and regeneration of **14a**. This step is endoergonic by 6.2 kcal mol^{-1}. In the following step, the reduction of (OCHO)Bpin to HCHO and (Bpin)O(Bpin), the substrate activation occurs by formation of a B–O bond between the N-ligated Bpin in **14b** and hydride transfer to the C atom of formoxyborane. The lowest energy key species in this step is a four-centered Mn–N–B–OCH_2-Bpin intermediate at −25.0 kcal mol^{-1}. The pathway proceeds by cleavage of the B–O bond, formation of a novel B–O–B bond and release of HCHO and **14a**. The final step, the reduction of HCHO to $(CH_3O)Bpin$, follows a similar sequence, with the highest barrier at 18.1 kcal mol^{-1}. Thermodynamic and kinetic analysis showed that the reduction reactivity follows the order HCHO > CO_2 > (OCHO)Bpin ≫ $(CH_3O)Bpin$.[34]

As an alternative study, in 2022 Cao, Lei and coworkers[35] approached the DFT study from a different point of view, *i.e.* by considering a possible inner-sphere activation mechanism involving prior Mn-CO bond dissociation, that was compared to a competitive outer-sphere carbonyl association mechanism involving N-ligated Bpin as in the previous study.[34] The CO dissociation mechanism involves the release of one CO ligand from **14a** to give a free coordination site that can in turn

coordinate the incoming substrate. The calculated results show that the highest barrier in the carbonyl association mechanism is 27.0 kcal mol^{-1}, corresponding to the hydride transfer step, while the rate-determining step of the carbonyl dissociation mechanism is the initial CO ligand release, with an energy barrier of 35.2 kcal mol^{-1}. Thus, the association mechanism was confirmed as the most accessible for this system.

Gonsalvi, Kirchner and coworkers described in 2020 the reduction of CO_2 to methoxyboranes catalyzed by the well-defined manganese complexes [MnX(PNP^{NR}-*i*Pr)(CO)$_2$] (R=H, X=H, **1 a**; R=Me, X=H, **1 b**; R=H, X=Br, **1 h**) shown in Figure 3, using HBpin and 9-BBN (9-BBN = 9-borabicyclo[3.3.1] nonane) as reductants and various organoborates as Lewis acids additives.[36] The best results using HBpin (2.24 mmol) or 9-BBN (1.12 mmol), CO_2 (1 atm), catalyst (0.05 mol %), $B(OPh)_3$ (10 mol %) in THF-d_6 at moderate temperature (60 °C), were obtained in the presence of complex **1 a**, with formation of (CH_3O)Bpin and (CH_3O)-9-BBN in 78 and 74% yield, respectively. Complexes **1 b** and **1 h** led to (CH_3O)Bpin in lower yields of 8% and 31% after 24 h, respectively. The formation of PhO-Bpin or PhO-9-BBN as side products of the reactions between boranes and $B(OPh)_3$ was observed. The proposed mechanism involves the initial activation of CO_2 by a putative highly electrophilic [Mn(PNP^{NH}–*i*Pr)(CO)$_2$][HB(OPh)$_3$] complex, suggested by the observation of a $^{31}P\{^1H\}$ NMR signal at 133.0 ppm during the test, allowing for the first kinetically sluggish reaction to give formoxyborane. Further reductions steps leading to the desired methoxyborane products were supposed to follow a metal-free reactivity in the presence of borane and the borate Lewis acid.

Later in 2023 Rong, Lei, Liu, De Proft and coworkers studied this system by DFT calculations.[37] Two possible mechanisms, involving ligand dearomatization (DA) and hydrogen transfer (HT), were considered (Scheme 17). As a common feature for the two mechanisms, HBpin is first activated in the initial step by metal-ligand cooperation, with the formation of a N–B bond and hydride transfer to Mn. For the DA mechanism, the highest barrier (14.6 kcal mol^{-1}) corresponds to the breaking of the B–N bond prior to release of (OCHO)Bpin, passing through transition state **TS1 d**. For the HT mechanism, each cycle involves hydrogen transfer between the substrate and the Bpin-N ligated active species, with the highest barrier at 17.2 kcal mol^{-1} corresponding to transition state **TS1 e**. Thus, the DA mechanism has a slightly lower barrier than HT in the CO_2 hydroboration to formoxyborane step. On the other hand, for the formaldehyde formation and formaldehyde hydroboration steps, HT is more favored than DA. The authors concluded that the overall reaction should be a mixture of these two mechanisms.

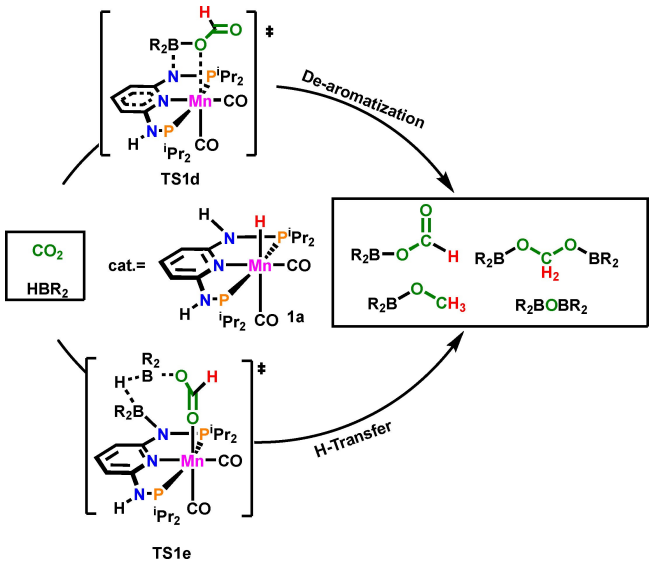

Scheme 17. Highest energy transition states in DA and HT mechanisms considered for CO_2 hydroboration with **1 a**. Reprinted (adapted) with permission from [37]. Copyright 2023 American Chemical Society.

Ghosh and Jacobi von Wangelin reported in 2021 the hydroboration of CO_2 with 100% selectivity to methoxyborane.[38] Rather low yields in (CH_3O)Bpin (21%, 20 h and 18%, 72 h) were obtained using [Mn(hmds)$_2$] (**15 a**) and [MnH(hmds)]$_6$ (hmds = hexamethyldisilazane) (**15 b**), respectively. The reactions were carried out in C_6D_6 under 1 bar CO_2, 80 °C, and 5 mol% catalyst. A catalytic cycle for the CO_2 hydroboration process was not proposed by the authors.

Gonsalvi, Kirchner and coworkers reported in 2023 on the selective reduction of CO_2 to boryl-protected MeOH in the presence of pinacolborane (HBpin) and well-defined, bench stable Mn(I) non-pincer-type complexes (**7**, **7 h–j**, Figure 3).[39]

Remarkably, complete hydroborane conversion and selective reduction to (CH_3O)Bpin was demonstrated in the absence of any base or additive. The best results were obtained with complexes **7** and **7 j** (1.0 mol % with respect to HBpin) in dmso-d_6 under very mild reaction conditions (60 °C, 1 bar CO_2, HBpin 0.224 mmol). Under these conditions, using **7** as a catalyst, (CH_3O)Bpin was obtained in very high yield (83%) after 1 h, that increased further after 24 h (99%). In case of **7 j** the reaction is faster and after 3 h full and selective conversion to methoxyborane was observed (yield = 100%). Formoxyborane was observed to form only in small amounts (ca. 6%) at the beginning of the reaction. In the case of complexes **7 h** and **7 i**, the reaction was much slower and after 24 h gave (CH_3O)Bpin in 76% (40 °C) and 12% yields (60 °C), respectively. The typical catalytic reaction was monitored by ^1H and $^{31}P\{^1H\}$ NMR, and the formation of various manganese complexes (**7 k–n**, Figure 4) was observed over time.

Complex **7 k** was then independently synthesized either by the reaction of **7** with HBpin (2 equiv) and dmso (2 equiv) in THF at 60 °C or upon heating a solution of **7 j** in dmso-d_6 to 40 °C. Complex **7 e** is characterized by ^1H NMR signals at

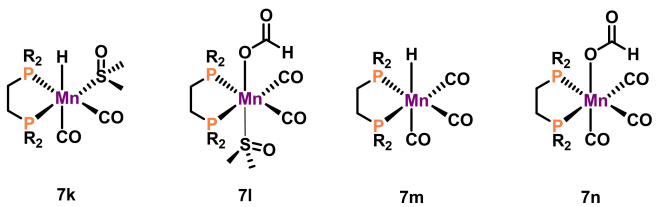

Figure 4. Manganese complexes **7 k–n** identified by NMR monitoring during CO_2 hydroboration runs in the presence of **8 a**.

−6.90 ppm (*t*, $^{2}J_{HP}$ = 49 Hz) and −7.02 ppm, (*t*, $^{2}J_{HP}$ = 49 Hz);^{31}P{^{1}H} NMR, δ = 120.9 ppm (d, $^{2}J_{PP}$ = 22 Hz), 105.2 ppm (d, $^{2}J_{PP}$ = 22 Hz). Complex **7l** was characterized as a singlet at 86.8 ppm in the ^{31}P{^{1}H} NMR monitoring, accompanied by a broad signal at 7.92 ppm in the corresponding ^{1}H NMR spectrum.

Complex **7m** was observed at 115.2 ppm in the ^{31}P{^{1}H} NMR spectra, and it was identified by comparison with literature data and independent synthesis. Finally, the ^{31}P{^{1}H} NMR signal at 89.5 ppm was tentatively attributed to complex *fac*-[Mn(κ^{1}-*O*-OCHO)(dippe)(CO)$_3$] (**7n**), that was separately obtained by reacting **7a** with formic acid.

4. CO_2 hydrosilylation

Another catalytic protocol applied for the homogeneous reduction of CO_2 is hydrosilylation. For this type of reaction, a wide library of hydrosilanes is commercially available, from mono- to bis- and tris-hydridosilanes, having different solubilities, electronic and steric properties. The use of hydrosilanes has the main advantage of replacing an explosive, pressurized gas such as hydrogen, and the lower energy required to activate the Si–H bond compared to the H–H bond. On the other hand, the principal drawback in CO_2 hydrosilylation is the need for highly chemoselective catalysts, in order to avoid the formation of mixtures of silyl formates, bis(silyl)acetals, methoxysilanes, bis(silyl)ethers, that in turn requires tedious purification and extraction (Scheme 1d). Whereas various reports are available in the literature for the selective synthesis of silyl formates, including many metal catalyzed protocols and recently a metal-free, solvent (DMSO, dimethylsulfoxide) promoted approach,[40] fewer examples describe the selective synthesis of methoxysilanes. These organosilane compounds can be of practical interest as methanol precursors, so their selective and efficient synthesis from abundant feedstocks such as CO_2 can be of interest.

To date, only two reports describe the use of Mn(I) organometallic catalysts for CO_2 hydrosilylation. In 2019, Gonsalvi, Kirchner and coworkers disclosed a detailed study on the application of the Mn-PN^{3}P complexes **1a** and **1b** as efficient, chemoselective catalysts for CO_2 hydrosilylation.[41] The selectivity of the reaction could be easily switched from silyl formates to methoxysilanes by simple tuning of the reaction conditions. After an initial solvent screening, confirming previous reports on the beneficial effects of DMSO for this type of reactions, the tests were run using $^{13}CO_2$ (1 bar), catalyst (0.014 mmol, catalyst:CO_2 = 1:10), $PhSiH_3$ (0.70 mmol, 5.0 equiv. Si–H bonds respect to CO_2, 2.0 mol% catalyst to Si–H bonds), DMSO-d_6 (400 μl) in J-Young type NMR tubes, monitoring the reactions by ^{13}C{^{1}H} NMR. At 25 °C, silyl formates were obtained with both catalysts in nearly quantitative yields after ca. 10 min. At longer reaction times (28–46 h), silyl formates were gradually converted to methoxysilanes in high yields (93%). The tests were repeated at 80 °C, obtaining selectively methoxysilanes in yields > 99% in the presence of **1a** after 6 h.

Having shown that highly efficient CO_2 utilization could be achieved, the tests were then run in Schlenk tube conditions using an excess of CO_2 to silanes, to gauge effective silane utilization. In a typical experiment, a Schlenk tube equipped with a Teflon Young valve (total volume = 15 mL) was charged with DMSO-d_6 (400 μL), $PhSiH_3$ (0.23 mmol; 0.7 mmol "Si–H", ca. 1 equiv. "Si–H" respect to CO_2), catalyst **1a** (0.007–0.014 mmol; 1 or 2 mol% respect to "Si–H") and CO_2 (1 bar). After 24 h at 80 °C, NMR analysis revealed the complete consumption of $PhSiH_3$ and 100% selective formation of methoxysilanes.

The catalytic mechanism involving **1a** was studied by DFT calculations, and the proposed catalytic cycle is shown in Scheme 18. The initial step involves the insertion of CO_2 into the Mn–H bond, resulting in the metal-coordinated formate [Mn{κ^{1}-*O*-(OCHO)}(PNP^{H}-*i*Pr)(CO)$_2$] (**1d**). This step requires to overcome a barrier of 8 kcal mol^{-1}. Then, a first silane molecule attacks the coordinated O-atom of formate in **1d**, transferring one hydride from Si to Mn, giving free silyl formate $(OCHO)SiH_2Ph$ with regeneration of **1a**. This step has the highest barrier of the entire path (29 kcal mol^{-1}). From this stage, the reaction follows by Mn–H attack onto the carbonyl C-atom of the silyl formate, generating [Mn{$(OCH_2O)SiH_2Ph$}(PNP^{H}-*i*Pr)(CO)$_2$] (**1i**), bearing a Mn-coordinated silyl hemiacetal ligand, with a barrier of 20 kcal mol^{-1}. The next step involves the attack of a second silane to the non-coordinated O-atom of the hemiacetal and the hydride transfer from the Si-atom to the carboxyl C-atom, liberating the silyl ether $(PhSiH_2)_2O$ and forming the Mn methoxo-complex [Mn(OCH_3)}(PNP^{H}-*i*Pr)(CO)$_2$] (**1j**). The step has a significant barrier (24 kcal mol^{-1}) but the process is however thermodynamically favored by a free energy balance gain of ΔG = −18 kcal mol^{-1}. Finally, a third silane molecule attacks the Mn-coordinated methoxide in **1j** and, transferring a hydride from Si to Mn, liberates $(CH_3O)SiH_2Ph$ and

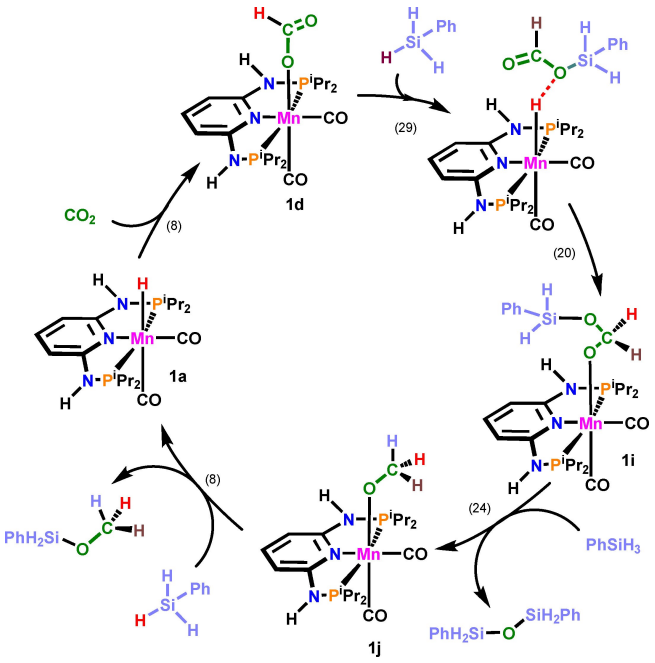

Scheme 18. Proposed catalytic cycle for CO_2 hydrosilylation to methoxysilane $(CH_3O)SiH_2Ph$ in the presence of **1a**. Energy barriers (kcal mol^{-1}) in brackets. Reprinted (adapted) with permission from [41]. Copyright 2019 American Chemical Society.

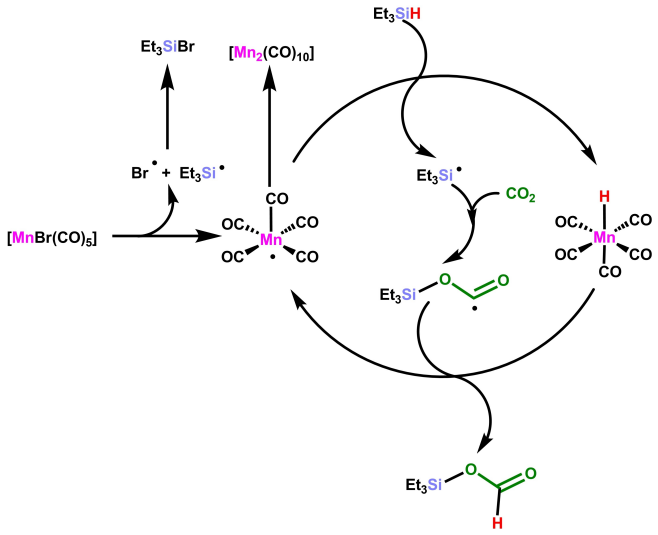

Scheme 19. Proposed catalytic cycle for CO_2 hydrosilylation to silyl formate $Et_3Si(OCHO)$ in the presence of $[MnBr(CO)_5]$. Reprinted from Ref. [42] with permission from Elsevier.

regenerates **1a**, with a barrier of only 8 kcal mol^{-1}. The calculations showed that the overall reaction is exergonic with $\Delta G = -28$ kcal mol^{-1}.

In 2021, Gonzalez and Garcia reported the use of $[MnBr(CO)_5]$ as an efficient pre-catalyst for CO_2 hydrosilylation with Et_3SiH as silane under mild reaction conditions.[42]

Using THF as a solvent, triethylsilylformate $Et_3Si(OCHO)$ was obtained in 67% yield after 1 h at 50 °C and CO_2 pressure (4 bar). By changing the solvent to a THF/toluene mixture, the bis(triethylsilyl)acetal $(Et_3SiO)_2CH_2$ was instead formed in 86% yield. At room temperature and atmospheric CO_2 pressure, the reaction still proceeded with high Et_3SiH conversions (92%–99%), albeit with a decrease in the selectivity, regardless of the solvent used. Radical species were proposed to be involved in the proposed catalytic mechanism (Scheme 19), based on radical trapping experiments.

5. Summary and Outlook

In summary, in this review article it has been shown that the use of an earth-abundant metal such as manganese can be relevant to the timely field of carbon dioxide reduction processes. Although this metal has received attention for this purpose only in the last decade, a growing number of catalytic studies are appearing in the literature. Key points for the successful implementation of Mn-based homogeneous processes, in view of the efficient replacement of the precious metal analogues, is the design of efficient metal-ligand architectures and choice of ancillary ligands. Pincer ligands are at the moment the most represented class, and outstanding results (total TON > 2000000) have been achieved by an evolutionary approach, for example in passing from PNP to PN^{3}P to PN^{5}P systems.

The success of pincer ligands resides in the easier synthetic tunability of the electronic and steric properties than other class of ligands, the ability to impart rigid meridional geometry to the complexes, in turn avoiding isomerization eventually leading to less active catalytic species, and the possible ligand participation in MLC-type substrate activation mechanisms. Some drawbacks are still to be solved, namely i) replacing expensive Mn precursors with cheaper analogues for the synthesis of the corresponding organometallic catalysts, and ii) achieving a better integration of predictive DFT calculations with experimental studies, to help avoiding time-consuming synthetic work leading to less interesting catalysts. In our opinion, the future studies should focus on the principal use of green H_2 as reductant, targeting more challenging products of (captured) CO_2 reduction, such as methanol and methane, to provide solutions for renewable, non-fossil based fuels, energy solutions and greenhouse gas control, based on the reuse of CO_2 as an abundant feedstock.

Acknowledgements

Recent research at CNR-ICCOM on the subject of the present review article was funded by the European Union – NextGeneration EU from the Italian Ministry of Environment and Energy Security POR H2 AdP MMES/ENEA with involvement of CNR and RSE, PNRR – Mission 2, Component 2, Investment 3.5 "Ricerca e sviluppo sull'idrogeno", CUP: B93 C22000630006, and the financial contribution is gratefully acknlowledged.

Conflict of Interests

The authors declare no conflict of interest.

Keywords: carbon dioxide · reduction processes · manganese complexes · homogeneous catalysis · mechanisms

[1] a) F. Nocito, A Dibenedetto, *Green Sustainable Chem.* **2020**, *21*, 34–43; b) S. Kar, A. Goeppert, G. K. S. Prakash, *Acc. Chem. Res.* **2019**, *52*, 2892–2903; c) *Carbon Dioxide Utilisation: Closing the Carbon Cycle*, 1st ed.; P. Styring, E. A. Quadrelli, K. Armstrong, Eds.; Elsevier, **2015**; d) G. Centi, G. Iaquaniello, S. Perathoner, *ChemSusChem* **2011**, *4*, 1265–1273; e) G. A. Olah, G. K. S. Prakash, A. Goeppert, *J. Am. Chem. Soc.* **2011**, *133*, 12881–12898.
[2] a) *CO_2 Hydrogenation Catalysis* (Ed.: Y. Himeda) Wiley-VCH, Weinheim, **2021**; b) *Chemical Transformations of Carbon Dioxide* (Eds: X. Wu, M. Beller), Topics in Current Chemistry Collections, Springer, **2018**; c) M. Aresta, A. Dibenedetto, A. Angelini, *Chem. Rev.* **2014**, *114*, 1709–1742.
[3] a) K. Rohmann, J. Kothe, M. W. Haenel, U. Englert, M. Hölscher, W. Leitner, *Angew. Chem. Int. Ed.* **2016**, *55*, 8966–8969; b) W. H. Wang, Y. Himeda, J. T. Muckerman, G. F. Manbeck, E. Fujita, *Chem. Rev.* **2015**, *115*, 12936–12973 and references therein; c) G. A. Filonenko, M. P. Conley, C. Copéret, M. Lutz, E. J. M. Hensen, E. A. Pidko, *ACS Catal.* **2013**, *3*, 2522–2526; d) J. F. Hull, Y. Himeda, W. H. Wang, B. Hashiguchi, R. Periana, D. J. Szalda, J. T. Muckerman, E. Fujita, *Nat. Chem.* **2012**, *4*, 383–388.
[4] L. Alig, M. Fritz, S. Schneider, *Chem. Rev.* **2019**, *119*, 2681–2751.
[5] a) Y. Zhang, A. D. MacIntosh, J. L. Wong, E. A. Bielinski, P. G. Williard, B. Q. Mercado, N. Hazari, W. H. Bernskoetter, *Chem. Sci.* **2015**, *6*, 4291–4299; b) R. Langer, Y. Diskin-Posner, G. Leitus, L. J. W. Shimon, Y. Ben-David, D. Milstein, *Angew. Chem. Int. Ed.* **2011**, *50*, 9948–9952.

[6] a) J. Schneidewind, R. Adam, W. Baumann, R. Jackstell, M. Beller, *Angew. Chem. Int. Ed.* **2017**, *56*, 1890–1893; b) M. S. Jeletic, M. T. Mock, A. M. Appel, J. C. Linehan, *J. Am. Chem. Soc.* **2013**, *135*, 11533–11536.
[7] B. G. Schieweck, N. F. Westhues, J. Klankermayer, *Chem. Sci.* **2019**, *10*, 6519–6523.
[8] S. Enthaler, J. von Langermann, T. Schmidt, *Energy Environ. Sci.* **2010**, *3*, 1207–1217.
[9] S. Kar, A. Goeppert, G. K. S. Prakash, Ch. 4 in *CO_2 Hydrogenation Catalysis*, (Ed.: Y. Himeda) Wiley-VCH, Weinheim, **2021**, pp. 89–112.
[10] a) J. Klankermayer, S. Wesselbaum, K. Beydoun, W. Leitner, *Angew. Chem. Int. Ed.* **2016**, *55*, 7296–7343; b) W.-H. Wang, X. Feng, M. Bao, Ch. 2, in *CO_2 Hydrogenation Catalysis*, (Ed.: Y. Himeda), Wiley-VCH, Weinheim, **2021**, pp. 13–52.
[11] K. S. Rawat, A. Mahata, I. Choudhuri, B. Pathak, *J. Phys. Chem. C* **2016**, *120*, 16478–16488.
[12] F. Bertini, M. Glatz, N. Gorgas, B. Stoger, M. Peruzzini, L. F. Veiros, K. Kirchner, L. Gonsalvi, *Chem. Sci.* **2017**, *8*, 5024–5029.
[13] A. Dubey, L. Nencini, R. R. Fayzullin, C. Nervi, J. R. Khusnutdinova, *ACS Catal.* **2017**, *7*, 3864–3868.
[14] S. Das, S. K. Pati, *Catal. Sci. Technol.* **2018**, *8*, 3034–3043.
[15] A. Kumar, P. Daw, N. A. Espinosa-Jalapa, G. Leitus, L. J. W. Shimon, Y. Ben-David, D. Milstein, *Dalton Trans.* **2019**, *48*, 14580–14584.
[16] K. Schlenker, E. G. Christensen, A. A. Zhanserkeev, G. R. McDonald, E. L. Yang, K. T. Lutz, R. P. Steele, R. T. VanderLinden, C. T. Saouma, *ACS Catal.* **2021**, *11*, 8358–8369.
[17] S. Kostera, S. Weber, M. Peruzzini, L. F. Veiros, K. Kirchner, L. Gonsalvi, *Organometallics* **2021**, *40*, 1213–1220.
[18] X. Chen, H. Ge, X. Yang, *Catal. Sci. Technol.* **2017**, *7*, 348–355.
[19] E. B. Hulley, K. D. Welch, A. M. Appel, D. L. DuBois, R. M. Bullock, *J. Am. Chem. Soc.* **2013**, *135*, 11736–11739.
[20] D. A. Kuß, M. Hölscher, W. Leitner, *ChemCatChem* **2021**, *13*, 3319–3323.
[21] D. A. Kuß, M. Hölscher, W. Leitner, *ACS Catal.* **2022**, *12*, 15310–15322.
[22] L. Zhang, M. Pu, M. Lei, *Dalton Trans.* **2021**, *50*, 7348–7355.
[23] C. Erken, A. Kaithal, S. Sen, T. Weyhermüller, M. Hölscher, C. Werlé, W. Leitner, *Nat. Commun.* **2018**, *9*, 4521.
[24] D. Wei, R. Sang, P. Sponholz, H. Junge, M. Beller, *Nat. Energy* **2022**, *7*, 438–447.
[25] K. S. Rawat, B. Pathak, *Catal. Sci. Technol.* **2017**, *7*, 3234–3242.
[26] C. M. Hert, J. B. Curley, S. P. Kelley, N. Hazari, W. H. Bernskoetter, *Organometallics* **2022**, *41*, 3332–3340.
[27] S. Kostera, G. Manca, L. Gonsalvi, *Chem. Eur. J.* **2023**, *29*, e202302642.
[28] S. Kar, A. Goeppert, J. Kothandaraman, G. K. S. Prakash, *ACS Catal.* **2017**, *7*, 6347–6351.
[29] S. C. Mandal, K. S. Rawat, S. Nandi, B. Pathak, *Catal. Sci. Technol.* **2019**, *9*, 1867–1878.
[30] J. Grover, S. Maji, C. Teja, S. A. A. Thabaiti, M. M. M. Mostafa, G. K. Lahiri, D. Maiti, *ACS Org. Inorg. Au* **2023**, *3*, 299–304.
[31] M. R. Espinosa, D. J. Charboneau, A. Garcia de Oliveira, N. Hazari, *ACS Catal.* **2019**, *9*, 301–314.
[32] T. Liu, W. Meng, Q.-Q. Ma, J. Zhang, H. Li, S. Li, Q. Zhao, X. Chen, *Dalton Trans.* **2017**, *46*, 4504–4509.
[33] S. Kostera, M. Peruzzini, L. Gonsalvi, *Catalysts* **2021**, *11*, 58.
[34] X. Wan, M. Li, R.-Z. Liao, *Chem. Asian J.* **2021**, *16*, 2529–2537.
[35] L. Zhang, Y. Zhao, C. Liu, M. Pu, M. Lei, Z. Cao, *Inorg. Chem.* **2022**, *61*, 5616–5625.
[36] S. Kostera, M. Peruzzini, K. Kirchner, L. Gonsalvi, *ChemCatChem* **2020**, *12*, 4625–4631.
[37] B. Wang, C. Rong, M. Lei, S. Liu, F. De Proft, *Inorg. Chem.* **2023**, *62*, 7366–7375.
[38] P. Ghosh, A. Jacobi von Wangelin, *Angew. Chem. Int. Ed.* **2021**, *60*, 16035–16043.
[39] S. Kostera, S. Weber, I. Blaha, M. Peruzzini, K. Kirchner, L. Gonsalvi, *ACS Catal.* **2023**, *13*, 5236–5244.
[40] H. Lv, Q. Xing, C. Yue, Z. Lei, F. Li, *Chem. Commun.* **2016**, *52*, 6545–6548.
[41] F. Bertini, M. Glatz, B. Stöger, M. Peruzzini, L. F. Veiros, K. Kirchner, L. Gonsalvi, *ACS Catal.* **2019**, *9*, 632–639.
[42] T. Gonzalez, J. J. Garcia, *Polyhedron* **2021**, *203*, 115242.

Manuscript received: October 31, 2023
Revised manuscript received: December 6, 2023
Accepted manuscript online: December 7, 2023
Version of record online: January 17, 2024